INVESTIGATION OF LATERAL ACCELERATION-BENDING COUPLING FOR A LARGE BOOSTER UTILIZING MULTI ACCELEROMETERS

FACILITY FORM 602

N66 24491
(ACCESSION NUMBER)

56
(PAGES)

CR-74551
(NASA CR OR TMX OR AD NUMBER)

1
(THRU)

(CODE)

32
(CATEGORY)

GPO PRICE $ _____

CFSTI PRICE(S) $ _____

Hard copy (HC) $3.00

Microfiche (MF) .50

ff 653 July 65

HAYES
INTERNATIONAL CORPORATION
BIRMINGHAM, ALABAMA



INVESTIGATION OF LATERAL ACCELERATION-BENDING COUPLING FOR A LARGE BOOSTER UTILIZING MULTI ACCELEROMETERS

ENGINEERING REPORT NO. 1213

22 DECEMBER 1965

PREPARED BY:

J. E. Bailey

S. R. McWaters

M. Frimer

APPROVED BY:

H. Passmore
Project Engineer

C. L. Anker
Project Manager

P. R. Coulson
Program Manager

REVISIONS

DATE	PAGES AFFECTED	REMARKS	BY	APP.

FORM E-509 REV. 2/3/61

ABSTRACT

24491

A method for analyzing lateral acceleration-bending coupling in a large flexible booster is studied with the hope of obtaining a simplified frequency domain analysis method which will aid in positioning multiple accelerometers. This analysis technique is an attempt to gain basic insight into the problem of positioning multiple accelerometers by defining a lateral-acceleration-bending filter function that depends on accelerometer position and number. The filter function amplitude and phase characteristic is varied by positioning the accelerometers.

Straightforward application of Nyquist criteria permits determination of the stability of the uncoupled bending-lateral acceleration loop. Trends in overall system stability are indicated by this technique as shown by comparison with root locus studies.

The method developed herein requires much less digital computer run time than comparable root locus studies and is applied to several familiar problems with some success.

Mr. R. S. Ryan, Chief, Dynamic Analysis Branch of the Flight Mechanics and Dynamics Division of the Aero-Astrodynamics Laboratory was the technical supervisor and the work reported herein was accomplished under contract NAS8-20201 with Marshall Space Flight Center, National Aeronautics and Space Administration.

Author

TABLE OF CONTENTS

TITLE	PAGE
LIST OF SYMBOLS	i
LIST OF FIGURES	iii
INTRODUCTION	1
THEORY	4
RESULTS	8
CONCLUSIONS	12
REFERENCES	13
APPENDIX	
AMPLITUDE PLOTS	
PHASE PLOTS	
NYQUIST DIAGRAMS	
ROOT CONTOURS	

LIST OF SYMBOLS

$\frac{A'}{I}$	System transfer function
A_i	Indicated lateral acceleration
A'	$g_{2\,i}\, A_i$
F_s	Swivel engine thrust
g	Longitudinal acceleration of the vehicle
$g_{2\,i}$	Gain of accelerometer control loop
i	The number of accelerometers
I	Effective moment of inertia of the vehicle about its c.g.
j	The number of bending modes
m_1 , m_2	Dynamic characteristics of engine gimbal system
M_{Bj}	Generalized bending mass
$P(\omega_n)$	The complex number found from $\frac{A'}{I}$ $(k\omega_n)$
X_{a_i}	Accelerometer location
Y	Translation displacement of rigid vehicle
Y_{ja_i}, Y'_{ja_i}	Displacement and slope of bending mode at X_{a_i}
Y_{jE}, Y'_{jE}	Displacement and slope of bending mode at X_E
β	Swivel angle (angle of the engine gimbal relative to the center line of the vehicle at the gimbal point)
β_c	Gimbal angle control signal

LIST OF SYMBOLS (CONTINUED)

ζ_{a_i}	Damping factor of accelerometer
ζ_{Bj}	Damping factor of bending mode
η_j	Generalized bending coordinate
ϕ	Pitch angle of rigid vehicle relative to inertial space
ω_{Bj}	Bending frequency (rad/sec)
ω_n	Coupled frequency

LIST OF FIGURES

FIGURE	TITLE	PAGE
1	LATERAL ACCELERATION-BENDING COUPLED SYSTEM	3
A	AMPLITUDE PLOTS FOR THREE BENDING MODES WITH ONE, TWO AND THREE ACCELEROMETERS	
A-1		14
A-2		17
A-3		20
A-4		24
A-5		27
A-6		30
A-7		34
A-8		37
A-9		40
B	PHASE PLOTS FOR THREE BENDING MODES WITH ONE, TWO AND THREE ACCELEROMETERS	
B-1		15
B-2		18
B-3		21
B-4		25
B-5		28
B-6		31

FIGURE	TITLE	PAGE
B-7		35
B-8		38
B-9		41
C	NYQUIST DIAGRAMS FOR THREE BENDING MODES WITH ONE, TWO AND THREE ACCELEROMETERS	
C-1		16
C-2		19
C-3		22
C-4		26
C-5		29
C-6		32
C-7		36
C-8		39
C-9		42
D-1	ROOT LOCUS FOR ONE, TWO AND THREE BENDING MODES WITH ACTUATOR DYNAMICS AND ONE ACCELEROMETER	23
D-2	ROOT LOCUS FOR ONE, TWO AND THREE BENDING MODES WITH ACTUATOR DYNAMICS AND TWO ACCELEROMETERS	33
D-3	ROOT LOCUS FOR ONE, TWO AND THREE BENDING MODES WITH ACTUATOR DYNAMICS AND THREE ACCELEROMETERS	43

TABLE	TITLE	PAGE
1	SUMMARY OF RESULTS SHOWING STABILITY AND INSTABILITY FOR VARIOUS ACCELEROMETER CONDITIONS	10

INTRODUCTION

The effects of bending coupling via the lateral acceleration loop of a large flexible booster vehicle is investigated for the purpose of defining sensor placement criteria for multiple accelerometers used in combination in the feedback loop. Past analysis of the multiaccelerometer, lateral acceleration feedback control problem at Hayes has been conducted with the aid of root locus plots of the system closed loop poles. The positions of multiple accelerometers were varied in systematic fashion and the variation in vehicle dynamics was observed on a root locus plot. The criterion for choosing sensor position was primarily based on stability of the overall system (sensors were varied to keep system poles in the left half plane). These studies pointed out several disadvantages of the method, which evaluated sensor position directly as a function of the closed loop system poles. First, all insight into the problem was lost. The basic mechanisms by which the acceleration-bending coupling affected stability of the various modes was not apparent. Second, the computational requirements were large due to the expansion of a high order determinant to obtain the characteristic equation which in turn had to be factored. This procedure was necessary for each sensor position and for a complicated system the computer time was extensive.

The purpose of this report is to investigate an alternate method for locating sensors, that would provide a good indication or estimate of optimum sensor positions, with a relatively small computational effort. The concept investigated herein which is used to accomplish this result, makes use of a bending-lateral

acceleration decoupling filter which is synthesized by positioning the multiple accelerometers which are combined to give the lateral acceleration feedback signal. A first try at this technique is attempted using a simplified vehicle model with no rigid body modes.

The simplified system developed herein includes gimbal dynamic, three bending modes, and mutliple accelerometers, with the rigid body modes omitted. With this set of simplified equations and a direct application of Nyquist criteria, an approximation of the effects of bending coupling via the lateral acceleration loop on system stability may be obtained. The advantage of this approach is that all system design may be accomplished with the open loop transfer functions. It must be realized that this is not a complete analysis of the bending coupling problem, but rather an accelerated procedure that provides an initial understanding of the problem.

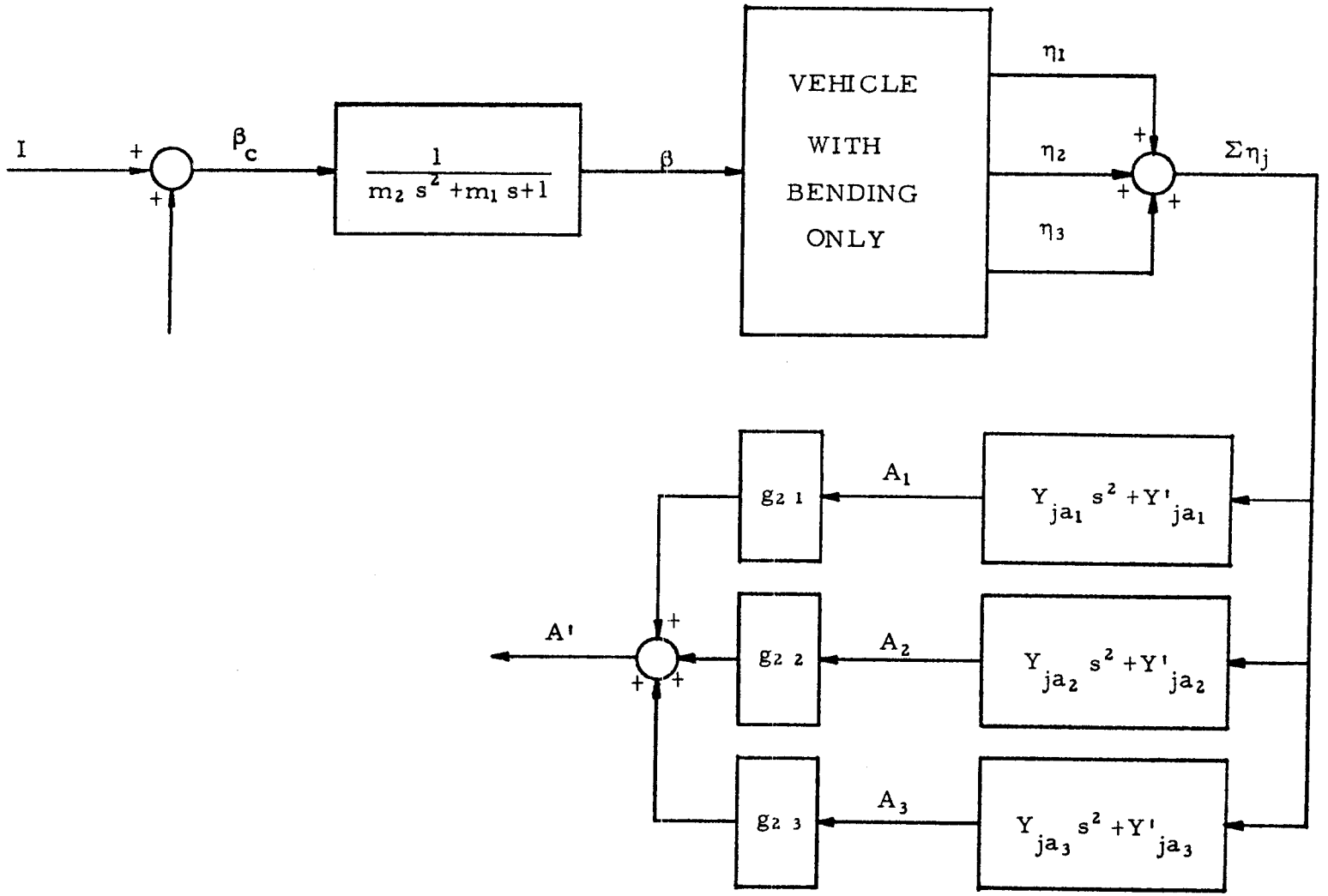


FIGURE 1. LATERAL ACCELERATION - BENDING COUPLED SYSTEM

THEORY

This analysis of lateral acceleration bending coupling will utilize a different approach for analyzing the interaction and coupling in the lateral acceleration loop. In brief, the accelerometer, bending mode, and gimbal dynamics equations will be used to examine the transfer characteristics through the bending equations and the lateral acceleration control loop as illustrated in Figure 1. It is helpful to think of the A'/I transfer function (frequency response function) as a lateral acceleration-bending mode coupling filter function which we may change at will by moving the relative position of the multiple accelerometers. The amplitude and phase characteristics of the A'/I transfer function will be investigated to determine to what degree they may be modified with various sensor placements and combinations.

Consider the following equations:

$$\ddot{\eta}_j + 2\zeta_{Bj}\omega_{Bj}\dot{\eta}_j + \omega_{Bj}^2\eta_j - \frac{F_s Y_{jE}}{M_{Bj}}\beta = 0 \qquad (1)$$

$$A_i - \ddot{Y} + X_{a_i}\ddot{\phi} + g\phi - \sum_j (Y_{ja_i}\ddot{\eta}_j + gY'_{ja_i}\eta_j) = 0 \qquad (2)$$

$$\beta_c - m_2\ddot{\beta} - m_1\dot{\beta} - \beta = 0 \qquad (3)$$

$$A' - \sum_i g_{2\,i} A_i = 0 \qquad (4)$$

where j = the number of bending modes and $_i$ = the number of accelerometers. The $\ddot{Y}$, $\ddot{\phi}$, and ϕ terms are omitted with the exclusion of the rigid body modes. This assumption is justified to some degree because the coupling between the bending modes and rigid body modes is small. Omission of the $\ddot{\phi}$ term is most significant. These simplifications are necessary to achieve the proper form of the A'/I transfer function and will be qualified later in the report.

The simplified Laplace transformed equations are

$$(S^2 + 2\zeta_{Bj}\omega_{Bj}S + \omega_{Bj}^2)\eta_j(S) = \frac{F_s Y_{jE}}{M_{Bj}} \beta \tag{1a}$$

$$A_i = \sum_j (Y_{ja_i} S^2 + g Y'_{ja_i}) \eta_j \tag{2a}$$

$$\beta_c = (m_2 S^2 + m_1 S + 1) \beta \tag{3a}$$

$$A'(S) - \sum_j g_{2\,i} A_i(S) = 0 \tag{4a}$$

The A'/β_c transfer function is defined as

$$\frac{A'(S)}{\beta_c(S)} = \left(\frac{A'(S)}{\eta_j(S)}\right) \left(\frac{\eta_j(S)}{\beta(S)}\right) \left(\frac{\beta(S)}{\beta_c(S)}\right) \tag{5}$$

Equation (5) is expanded to give

$$\frac{A'(S)}{I(S)} = \sum_i \sum_j \frac{g_{2i}\left[Y_{ja_i} S^2 + gY'_{ja_i}\right] \frac{F_s Y'_{jE}}{M_{Bj}}}{(m_2 S^2 + m_1 S + 1)(S^2 + 2\zeta_{Bj}\omega_{Bj} S + \omega_{Bj}^2)} \qquad (6)$$

when $\beta_c = 1$, which is the open loop transfer function for the lateral acceleration-bending loop.

The frequency response function for the lateral acceleration-bending loop is obtained by the substitution $S = k\omega$ in equation 6. The frequency response function is

$$\frac{A'(k\omega)}{I(k\omega)} = \sum_i \sum_j \frac{g_{2i}\left(\frac{F_s Y_{jE}}{M_{Bj}}\right)\left(-\omega^2 Y_{ja_i} + gY'_{ja_i}\right)}{\left[m_2\omega^4 - (m_2\omega_{Bj} + 2\zeta_{Bj}\omega_{Bj}m_1 + 1)\omega^2 + \omega_{Bj}\right]} + k\left[-(2\zeta_{Bj}\omega_{Bj}m_2 + m_1)\omega^3 + (m_1\omega_{Bj} + 2\zeta_{Bj}\omega_{Bj})\omega\right] \qquad (7)$$

where $k = \sqrt{-1}$.

For computational purposes we will define

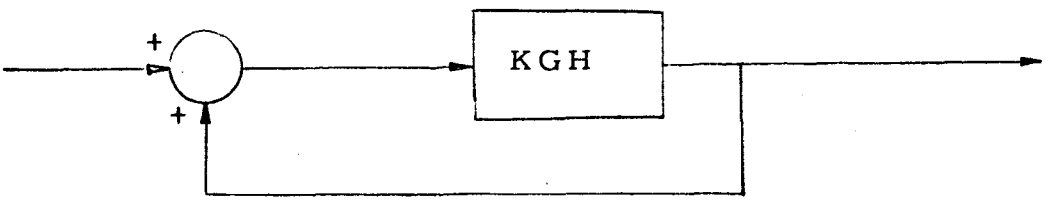
$$P(\omega) = \left|P(\omega)\right| e^{k\theta} = \frac{A'}{I}(k\omega)$$

The complex number $P(\omega)$ computed from equation (7) presents a complete picture of the amplitude and phase of the lateral acceleration-bending coupling at each frequency ω. The computation of $P(\omega)$ requires relatively small digital computer computational time and makes investigation of effects of large numbers

of accelerometers and bending modes feasible.

Two methods of analysis are feasible: (1) Analysis of amplitude and phase plots of P (Bode plots) to determine ability to shape P by moving accelerometers. (2) Analysis of loop stability using Nyquist criteria. Both methods may be compared with root locus plots for the unsimplified system equations to validate results obtained from the simplified analysis.

The Generalized Nyquist Criteria was applied to the system as defined below



where the sign of K is determined by the sign of Y_{ja_i} and Y'_{ja_i}, the displacement and slope respectively of the j-th bending mode at the i-th accelerometer position. Note that the system is assumed to have positive feedback and the resulting criterion for stability of this system is zero encirclements of the (1, 0) point. Variations in the sign of K appear implicitly in the Nyquist diagram. The system in question has no open loop poles in the right half plane as evidenced by inspection of equation (6).

RESULTS

In order that the feasibility of the technique previously described can be investigated, three separate booster control system configurations were investigated. The cases chosen are as follows:

(1) Booster model with three bending modes and one accelerometer in the lateral acceleration feedback loop.

(2) Same as (1) except with 2 accelerometers combined to give A_1.

(3) Same as (1) except with 3 accelerometers combined.

Both good and bad accelerometer locations for the above mentioned cases were chosen from previous analysis of the problem. Root locus plots illustrating the effect of accelerometer position on system closed loop poles is presented in Figures D-1, D-2, and D-3 for cases 1, 2, and 3. For this study the static acceleration feedback gain g_2 for the drift minimum case ($g_2 = .038667$) was used in conjunction with nominal values of a_1 and a_0. When multiple accelerometers are used the static contribution of all sensors is chosen to give $g_2 = .038667$ with equal weight given to each accelerometer.

The $P(\omega)$ data for the three cases is presented in two forms. First amplitude and phase plots (for various accelerometer positions) are shown in Figures A-1 through B-9. Next Nyquist plots of $P(\omega)$ for the various cases are presented in Figures C-1 through C-9. Both the Bode plots and the Nyquist plots can be correlated with the root locus plots for the nonsimplified system.

With the aid of the Bode and Nyquist plots we will now try to answer the following questions in order that some light may be shed on the usefulness of this technique:

(1) Is there correlation between nonsimplified system stability as indicated in the root locus plots and the simplified system Nyquist diagrams?

(2) How much modification of the filter function $P(\omega)$ is feasible, and can the modifications be used as a quantitative indication of system stability? Can improvements be noted quantitatively on the Bode plots?

(3) Can this method be used successfully as a tool for positioning multiple accelerometers.

First, question (1) will be discussed in view of the root locus and Nyquist plots. The following table presents these results at a glance:

From Table 1 it can be seen that the simplified system Nyquist plot predicts in general very stable and very unstable cases with fair accuracy. However, marginally stable (roots close to imaginary axis) system characteristics are not predicted well. These results are in general what is to be expected from a simplification of the type in question. Normally we would expect the simplified system to be more stable than the nonsimplified system. Tentatively it can be said, in answer to question (1) that there is correlation between the simplified system and the nonsimplified.

In answer to question (2), we will refer to the Bode plots of $P(\omega)$ shown in Figures A-1 through A-9. Inspection of the amplitude plots of $P(\omega)$ immediately show a very marked similarity in shape, with the main difference being a reduction in overall level of $P(\omega)$ as the number of accelerometers is increased. Good location of either one, two, or three accelerometers seems to give a very similar shape $P(\omega)$ versus ω curve. However, good location of 3 accelerometers

CASE I ONE ACCELEROMETER			CASE II TWO ACCELEROMETERS			CASE III THREE ACCELEROMETERS		
X_A	ROOT LOCUS NONSIMPLIFIED	NYQUIST SIMPLIFIED	X_{A_1}	ROOT LOCUS NONSIMPLIFIED	NYQUIST SIMPLIFIED	X_{A_1}	ROOT LOCUS NONSIMPLIFIED	NYQUIST SIMPLIFIED
-3	STABLE	STABLE	1	STABLE	STABLE	9	STABLE	STABLE
-11	ONE MODE SLIGHTLY UNSTABLE	MARGINAL STABILITY	9	ONE MODE MARGINAL AND ONE UNSTABLE	STABLE	5	MARGINAL STABILITY	STABLE
-47	UNSTABLE	UNSTABLE	-23	UNSTABLE	UNSTABLE	-3	UNSTABLE	MARGINALLY STABLE

TABLE 1 SUMMARY OF RESULTS SHOWING STABILITY AND INSTABILITY FOR VARIOUS ACCELEROMETER CONDITIONS

markedly reduces the amplitude of $P(\omega)$. The phase plots shown in Figures B-1 through B-9 exhibit very similar characteristics and correlate well with trends indicated by the Nyquist plots. Radical phase changes are seen to correspond to unstable cases predicted by the nonsimplified equations. Movement of the accelerometer positions gives in some instances major changes in the filter function phase characteristic. In answer to question (2) we will conclude (1) that great changes in the filter function $P(\omega)$ do not seem feasible but significant changes in phase can be produced. (2) Quantitative stability information is not directly obtainable from the Bode plots; however, good accelerometer locations seem to give a particular shape of filter function amplitude and phase. Qualitative information does exist, however, but more cases need to be considered before the Bode plot information is very useful.

In answer to question (3) which concerns the feasibility of using this technique as a design tool we will have to say that more work needs to be done before direct use can be made of this method. If used as supplementary design information the method as presented herein will provide useful results in the form of approximate accelerometer locations. It should be remembered that this method is approximate and the effect of the $X_{a_i}\ddot{\phi}$ term in the equations needs to be considered separately. From previous studies it is indicated that $\sum_i X_{a_i}$ should equal zero.

CONCLUSIONS

The major conclusions resulting from this study are as follows:

1. In general, the simplified method for choosing accelerometer positions was successful in predicting system stability, as the comparison with root locus studies indicate.

2. It is concluded that major shaping of the filter function can be obtained by accelerometer position variation and these results can be directly translated into qualitative information regarding sensor placement.

3. Quantitative stability information is not obtainable from the results of this analysis.

4. Major savings in computer time were achieved by using this technique for analysis of multiple sensor location effects.

It is generally concluded from this study that an approach of this type is feasible and could concievably be a very useful tool for sensor positioning.

REFERENCES

1. Cheng, David K., "Analysis of Linear Systems", Addison-Wesley Publishing Company, Inc., Reading, Massachusetts, 1959.

2. McWaters, S. Rex and Bailey, J. E., "Stability Investigation of Multi-Accelerometer Control of Large Flexible Booster Vehicles", Hayes Engineering Report No. 1054 , Birmingham, Alabama, 20 August 1964.

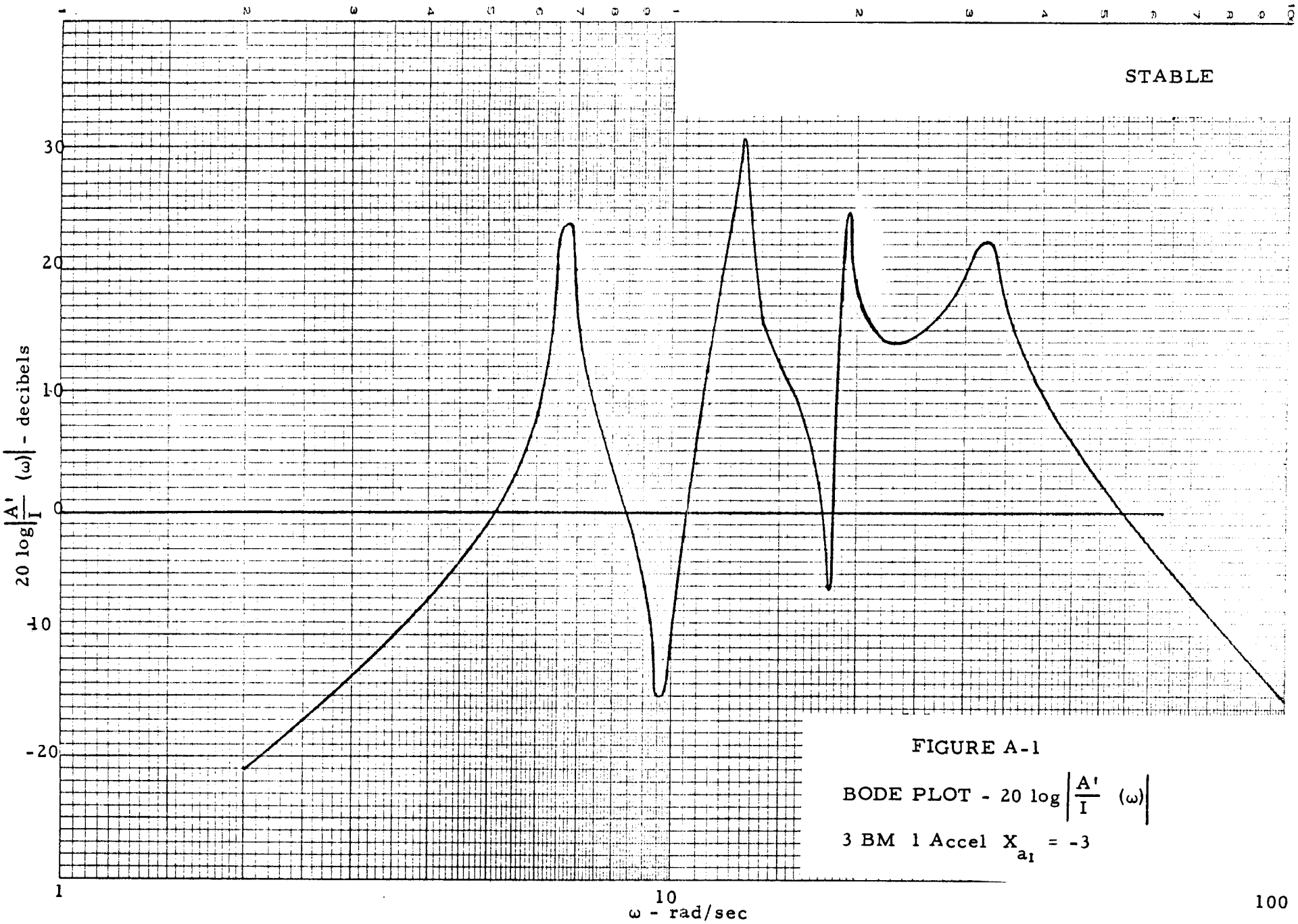


FIGURE A-1

BODE PLOT - $20 \log \left| \frac{A'}{I} (\omega) \right|$

3 BM 1 Accel $X_{a_1} = -3$

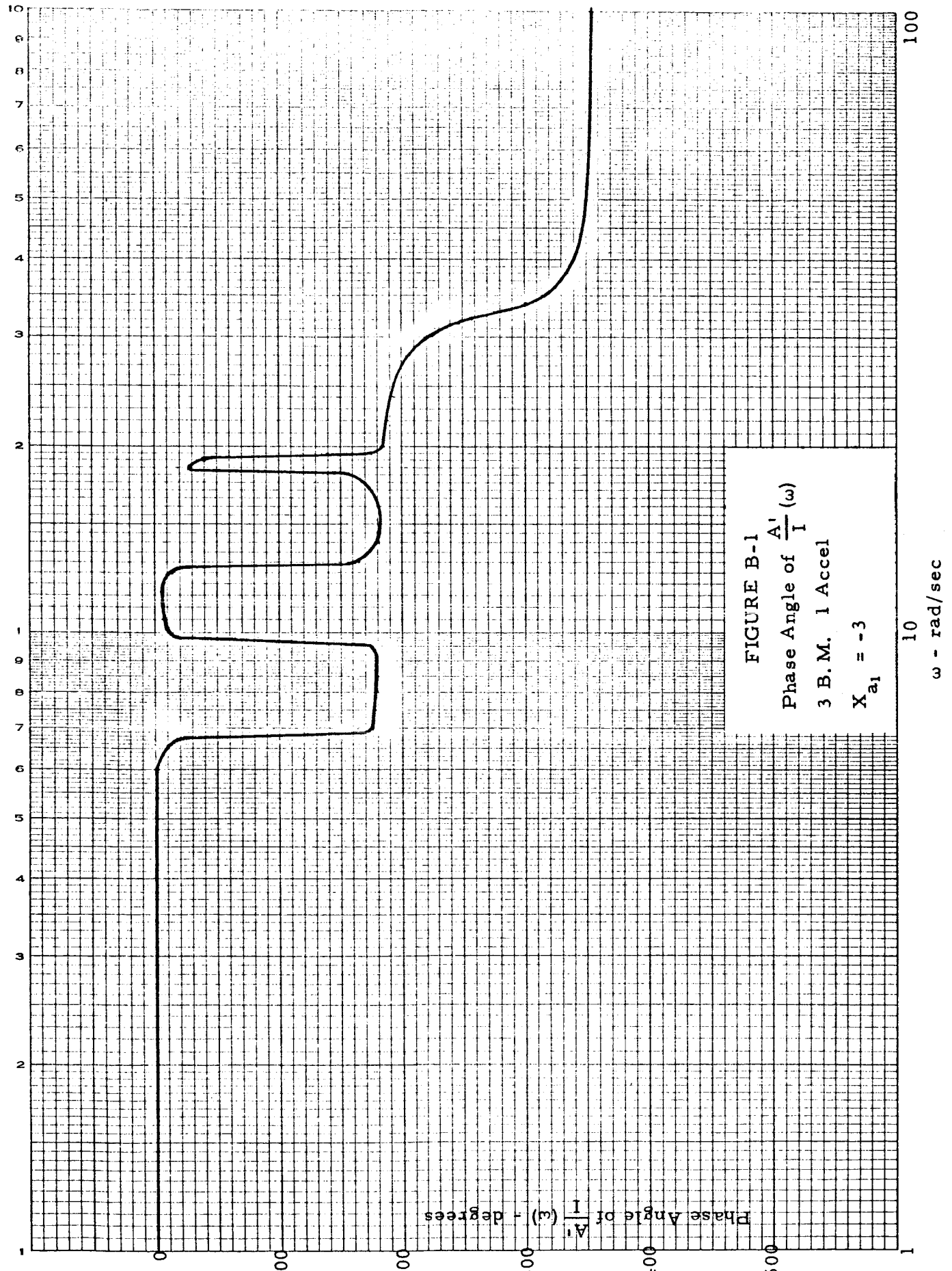


FIGURE B-1
Phase Angle of $\frac{A'}{I}(\omega)$
3 B.M. 1 Accel
$X_{a_1} = -3$

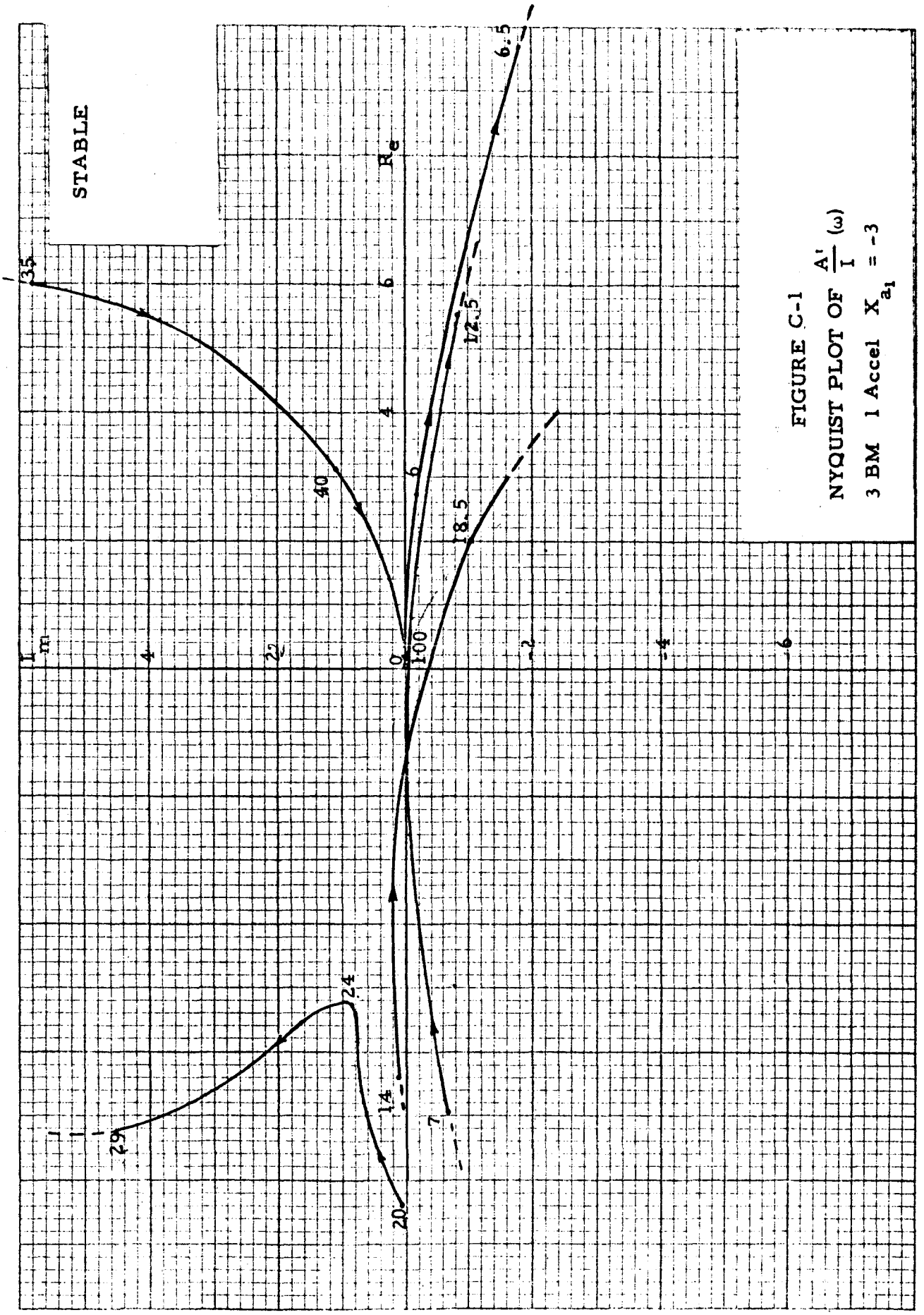


FIGURE C-1
NYQUIST PLOT OF $\frac{A'}{I}(\omega)$
3 BM 1 Accel $X_{a_1} = -3$

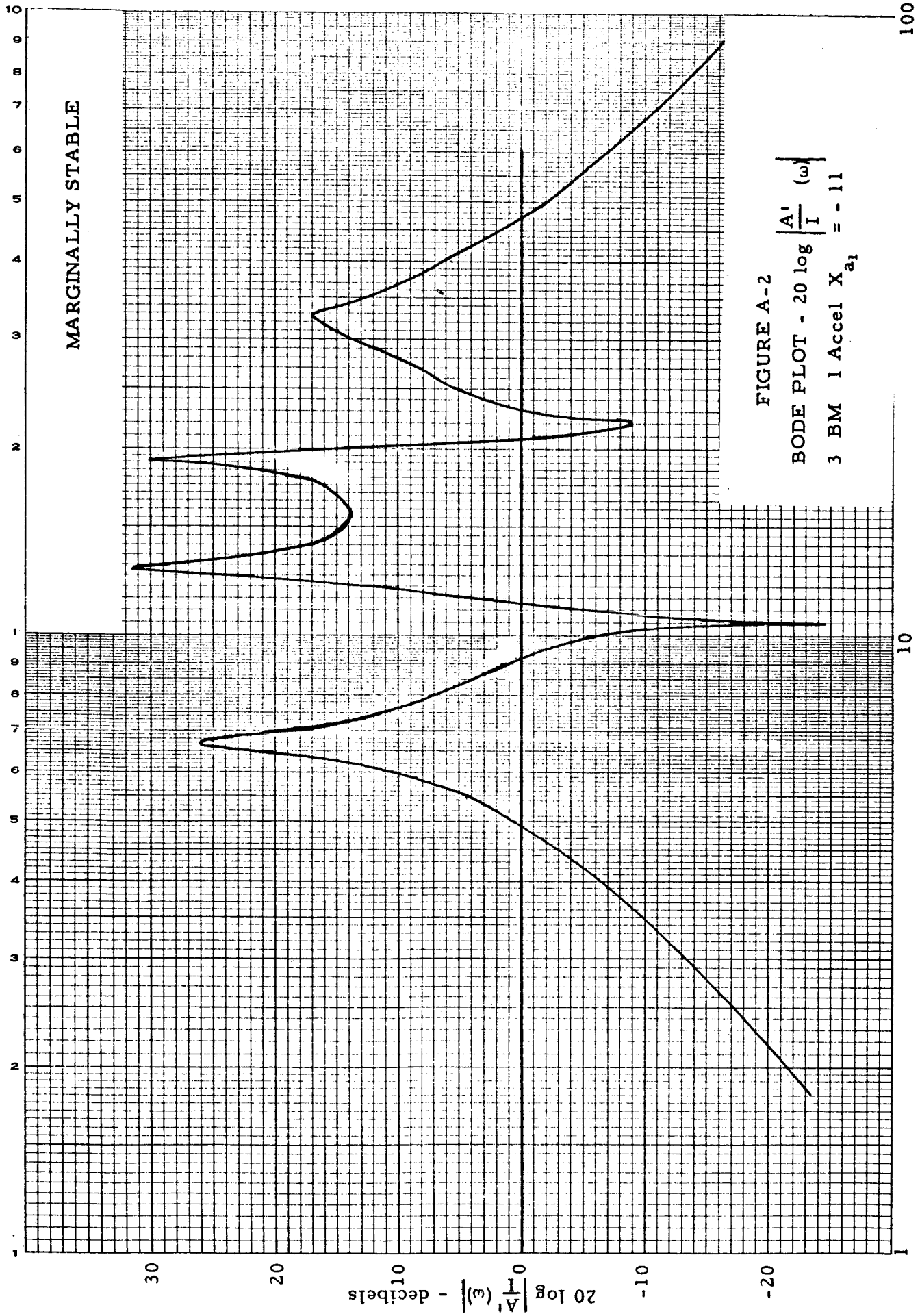


FIGURE A-2
BODE PLOT - 20 log $\left|\frac{A'}{T}(\omega)\right|$
3 BM 1 Accel X_{a_1} = - 11

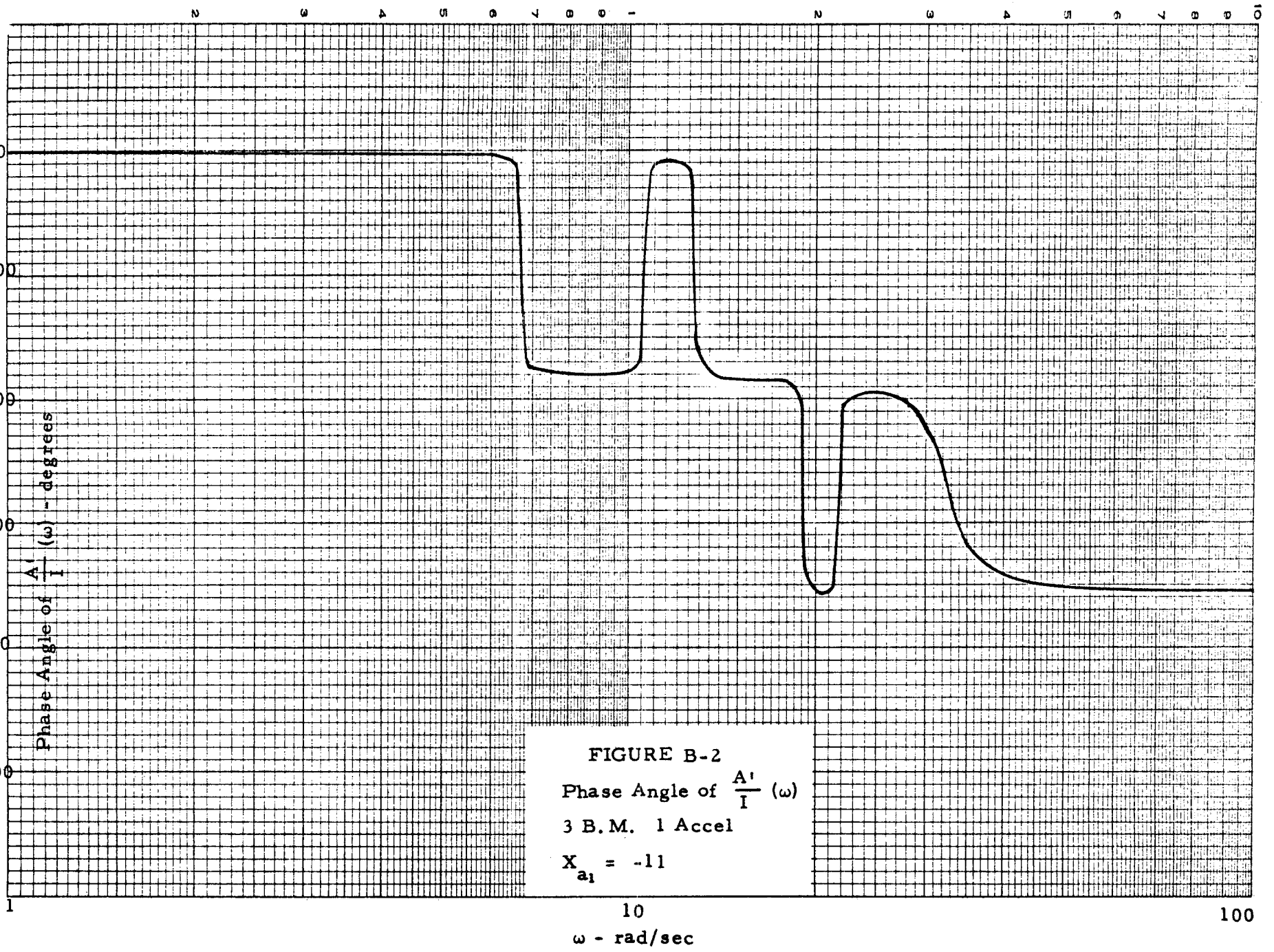


FIGURE B-2

Phase Angle of $\frac{A'}{I}$ (ω)

3 B.M. 1 Accel

X_{a_1} = -11

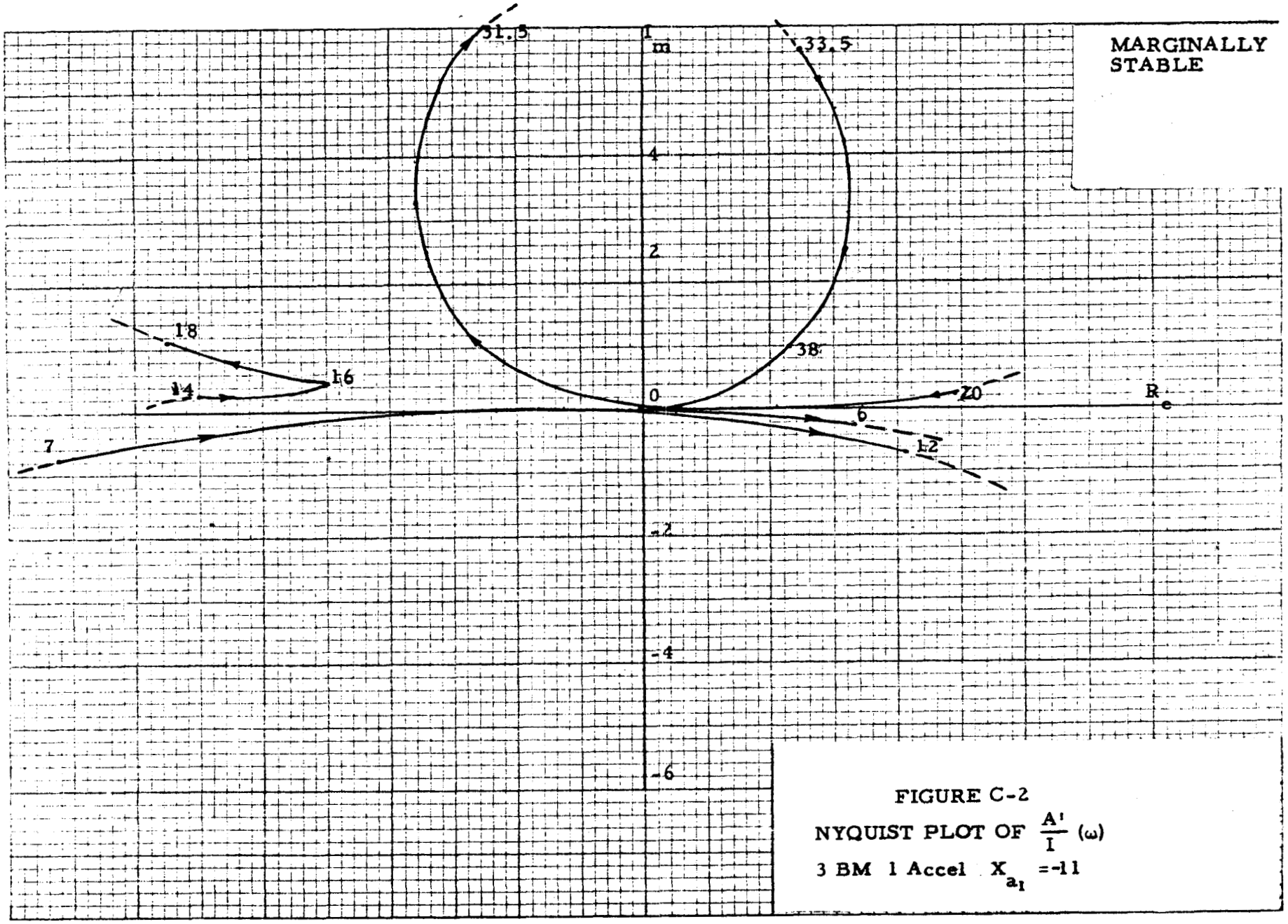
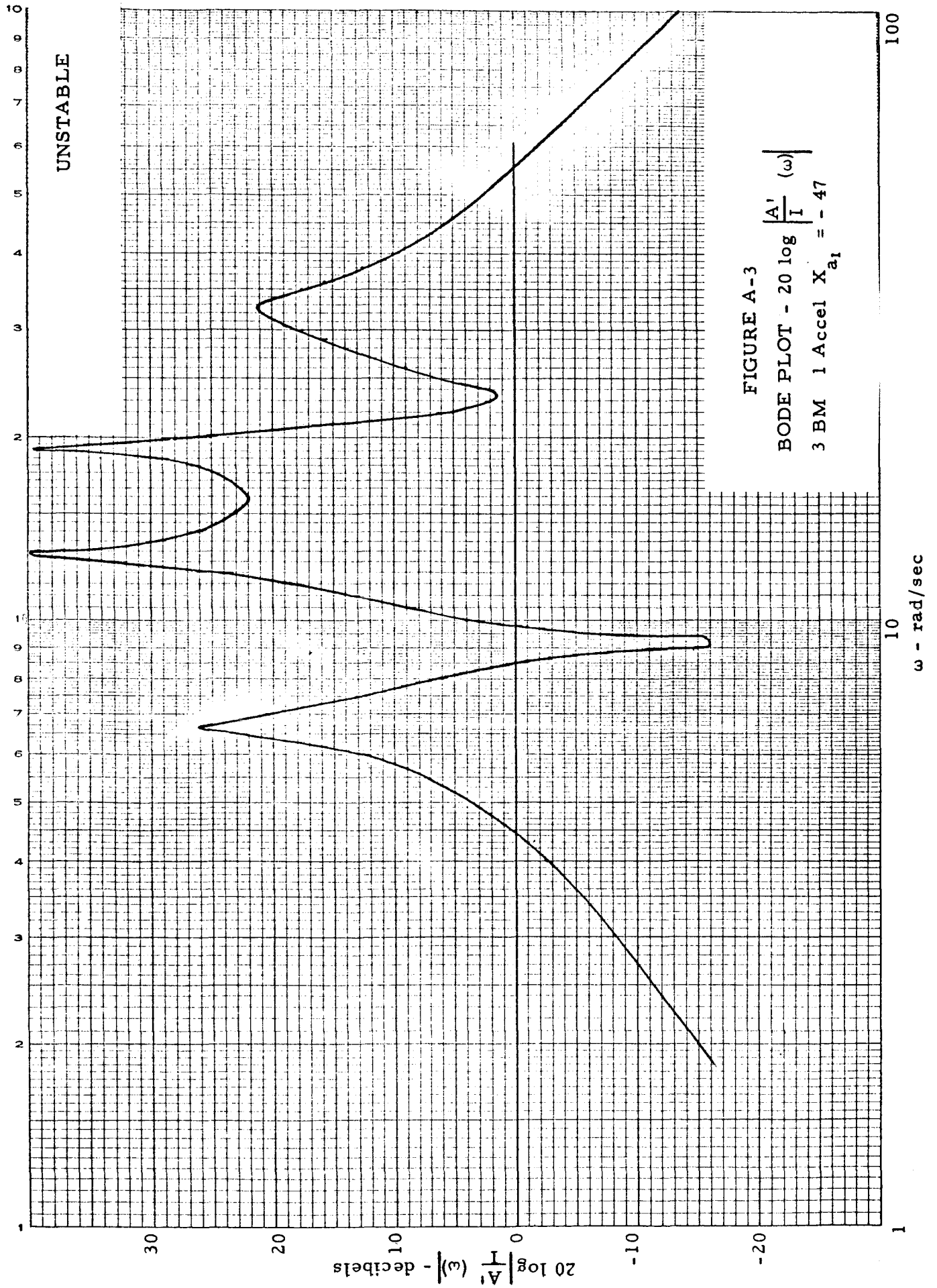
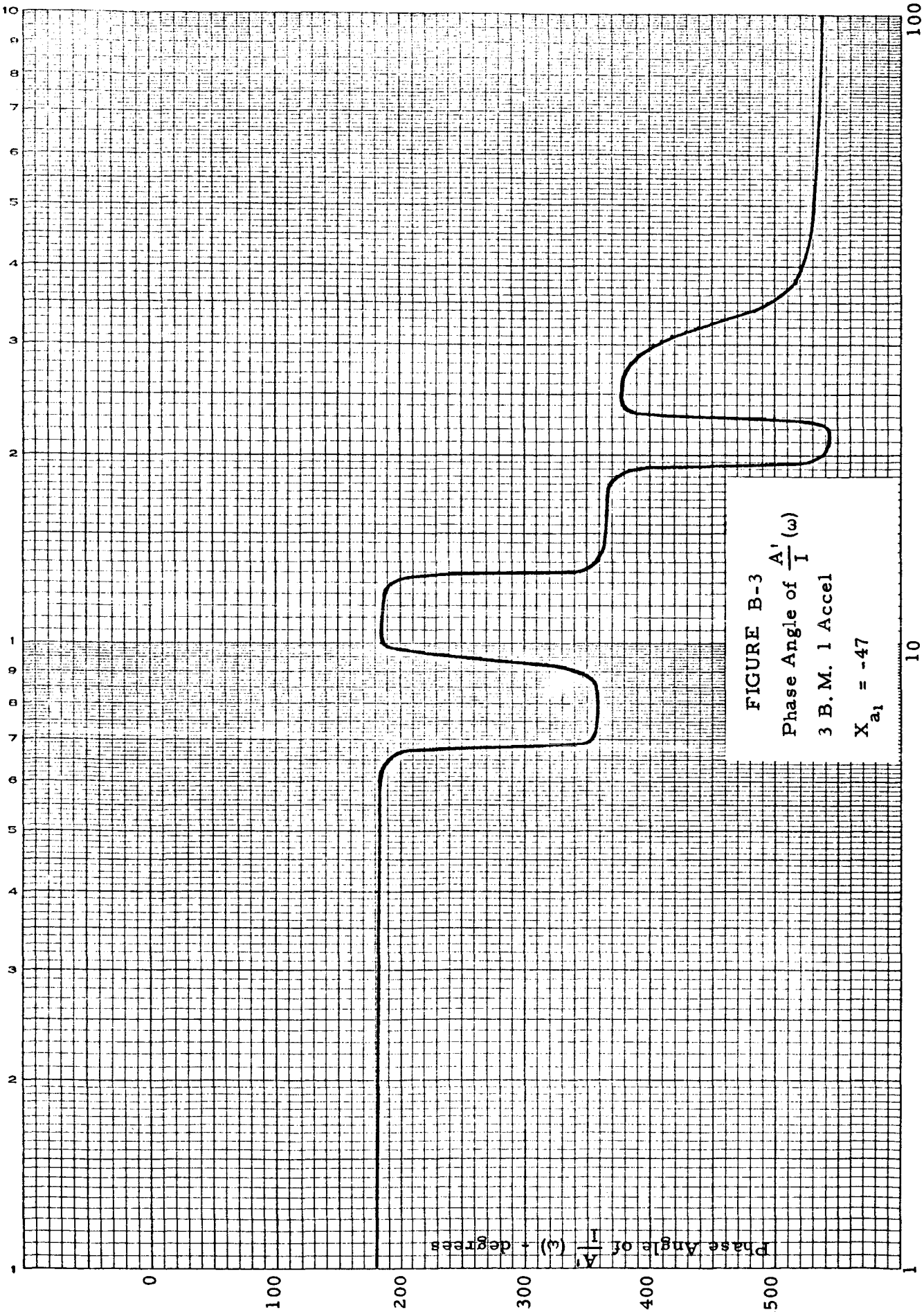


FIGURE C-2

NYQUIST PLOT OF $\frac{A'}{I}(\omega)$

3 BM 1 Accel X_{a_1} =-11


UNSTABLE
FIGURE A-3
BODE PLOT - 20 log |A'/I (ω)|
3 BM 1 Accel X_a1 = - 47
20 log |A'/I (ω)| - decibels
ω - rad/sec
30
20
10
0
-10
-20
1
2
3
4
5
6
7
8
9
10
100


Phase Angle of $\frac{A'}{I}$ (ω) - degrees
0
-100
-200
-300
-400
-500
1
2
3
4
5
6
7
8
9
10
100
ω - rad/sec
FIGURE B-3
Phase Angle of $\frac{A'}{I}$ (ω)
3 B.M. 1 Accel
X_{a_1} = -47

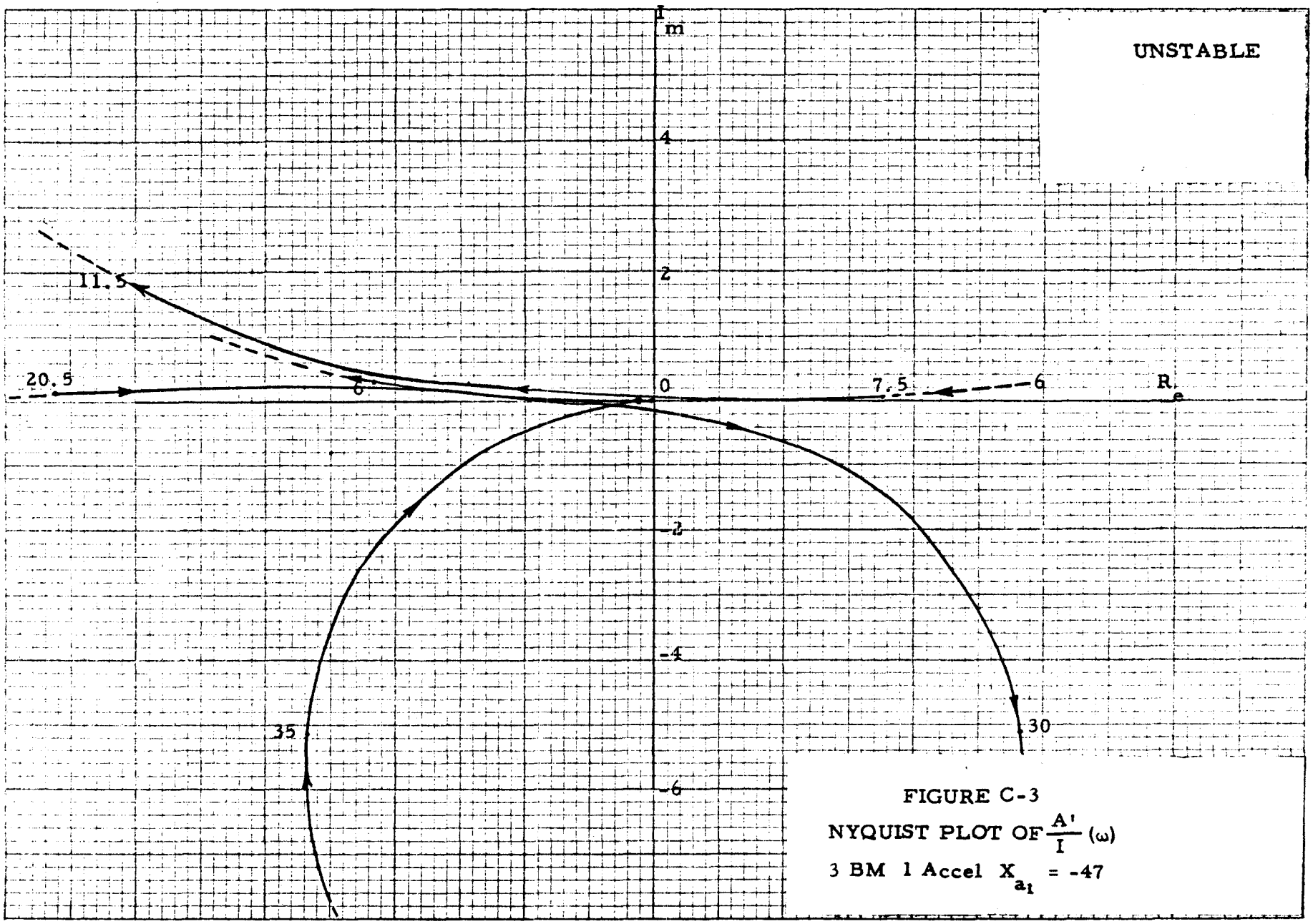


FIGURE C-3

NYQUIST PLOT OF $\frac{A'}{I}(\omega)$

3 BM 1 Accel $X_{a_1} = -47$

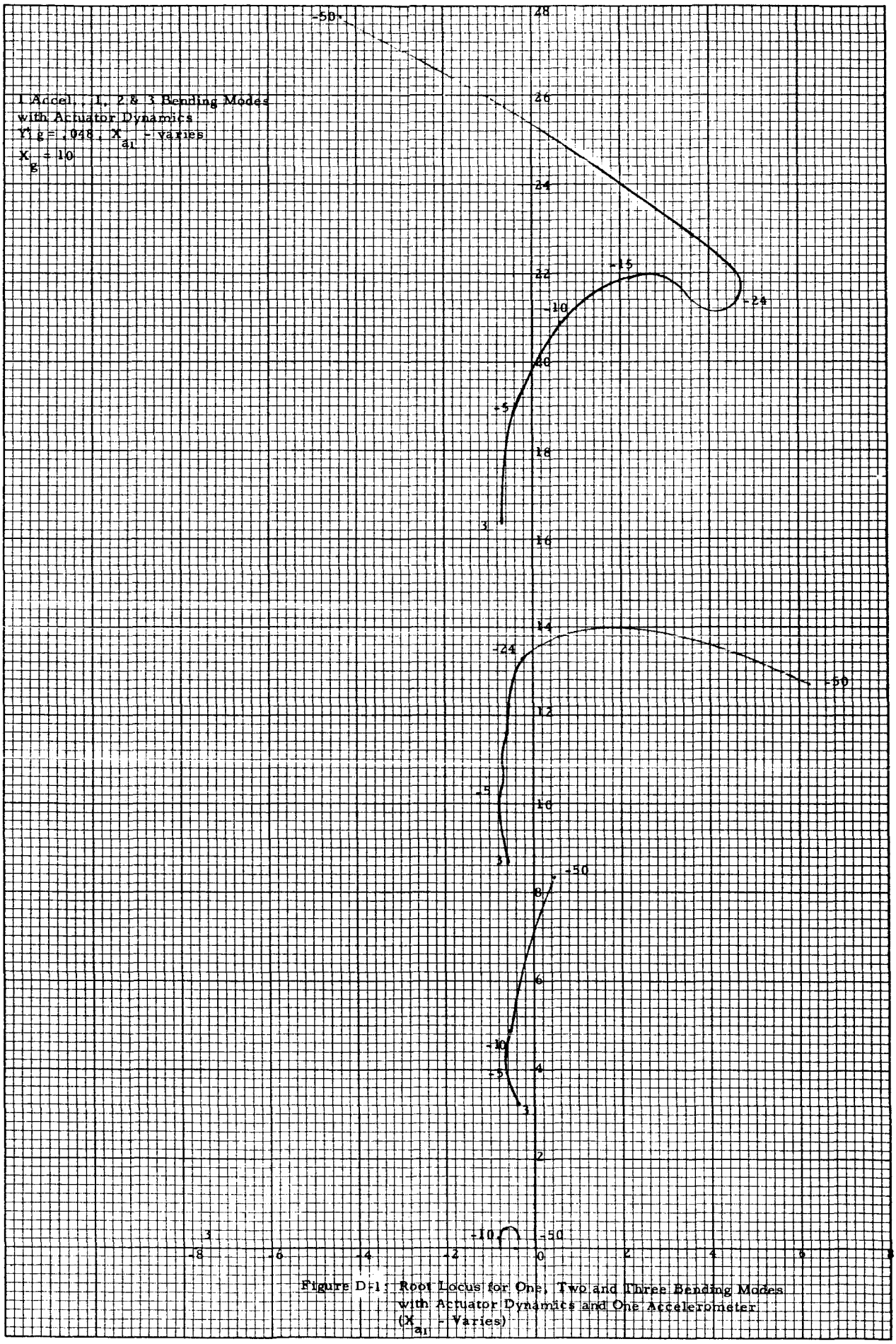


Figure D-1: Root Locus for One, Two and Three Bending Modes with Actuator Dynamics and One Accelerometer (X_{ai} - Varies)

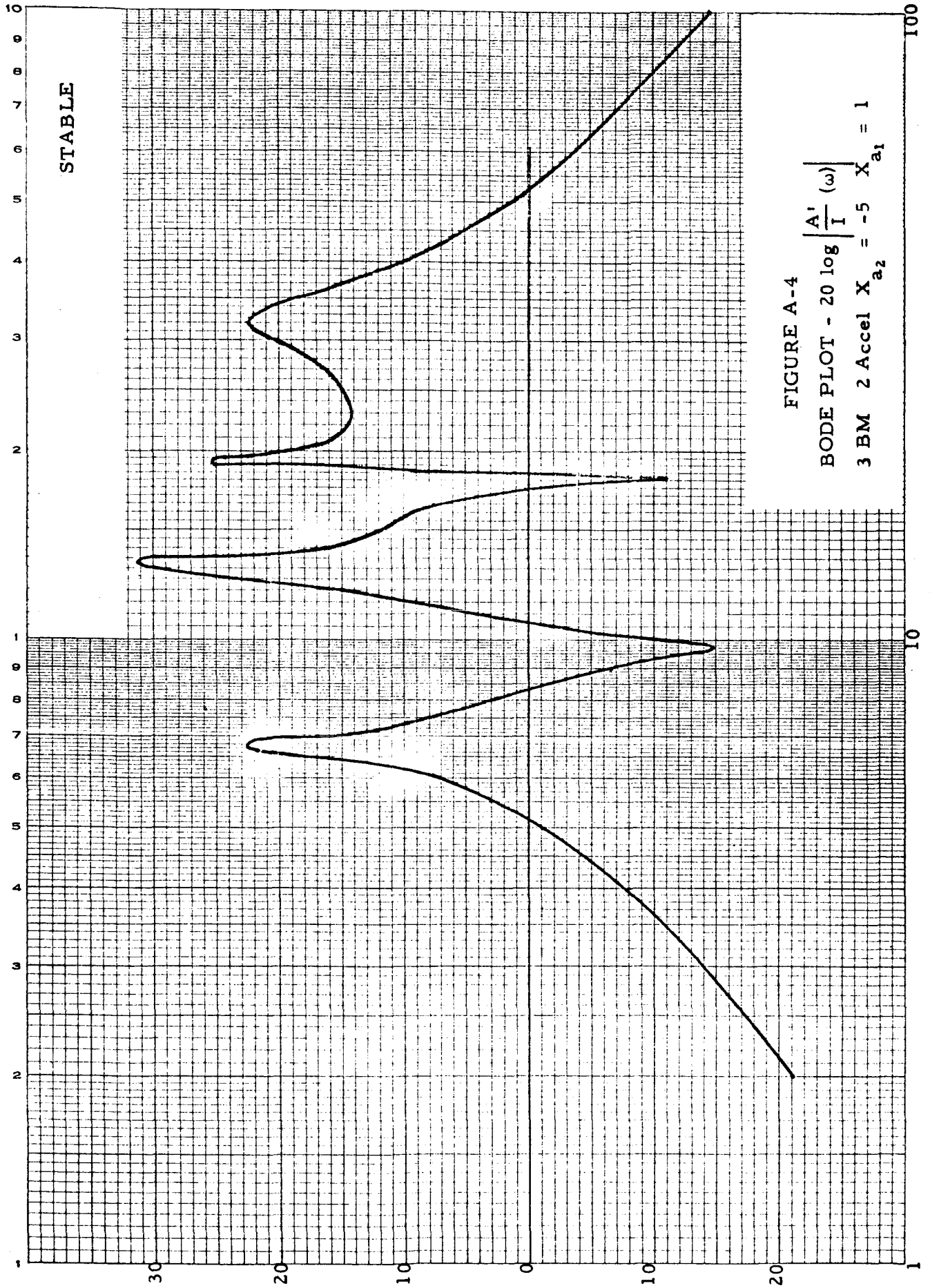


FIGURE A-4
BODE PLOT - $20 \log \left| \frac{A'}{I} (\omega) \right|$
3 BM 2 Accel $X_{a_2} = -5$ $X_{a_1} = 1$

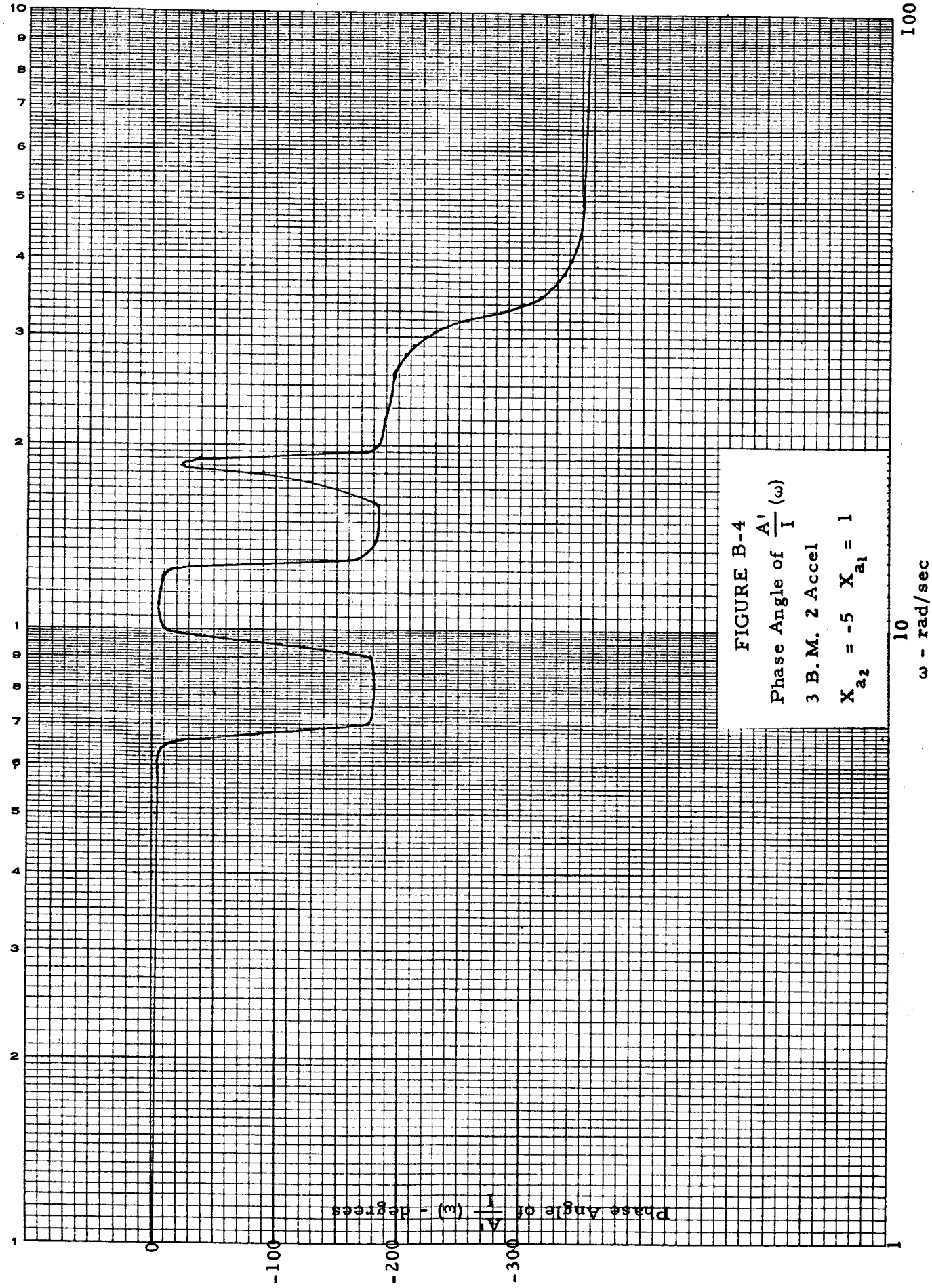


FIGURE B-4
Phase Angle of $\frac{A'}{I}(\omega)$
3 B.M. 2 Accel
$X_{a_2} = -5 \quad X_{a_1} = 1$

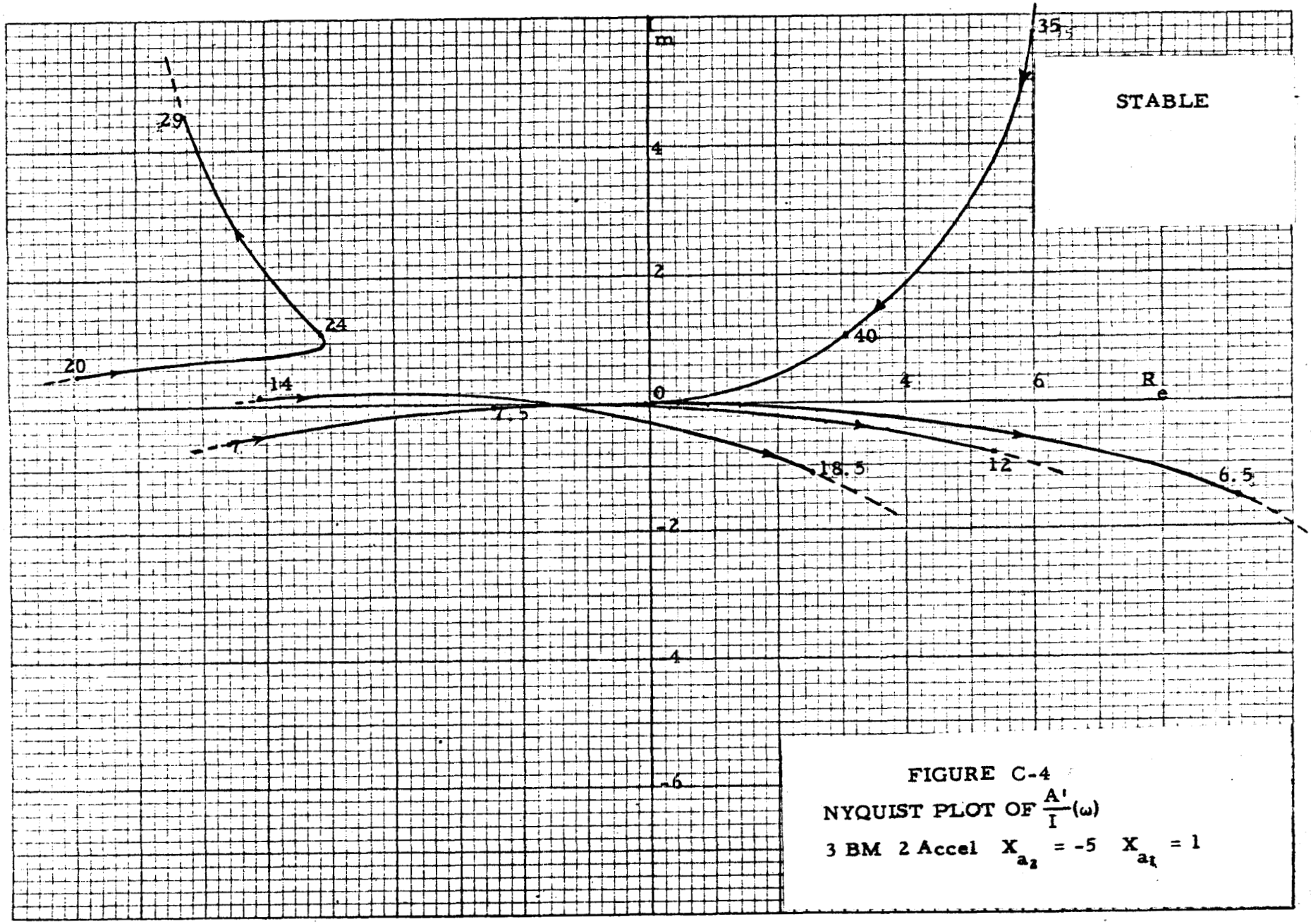


FIGURE C-4

NYQUIST PLOT OF $\frac{A'}{I}(\omega)$

3 BM 2 Accel $X_{a_2} = -5$ $X_{a_1} = 1$

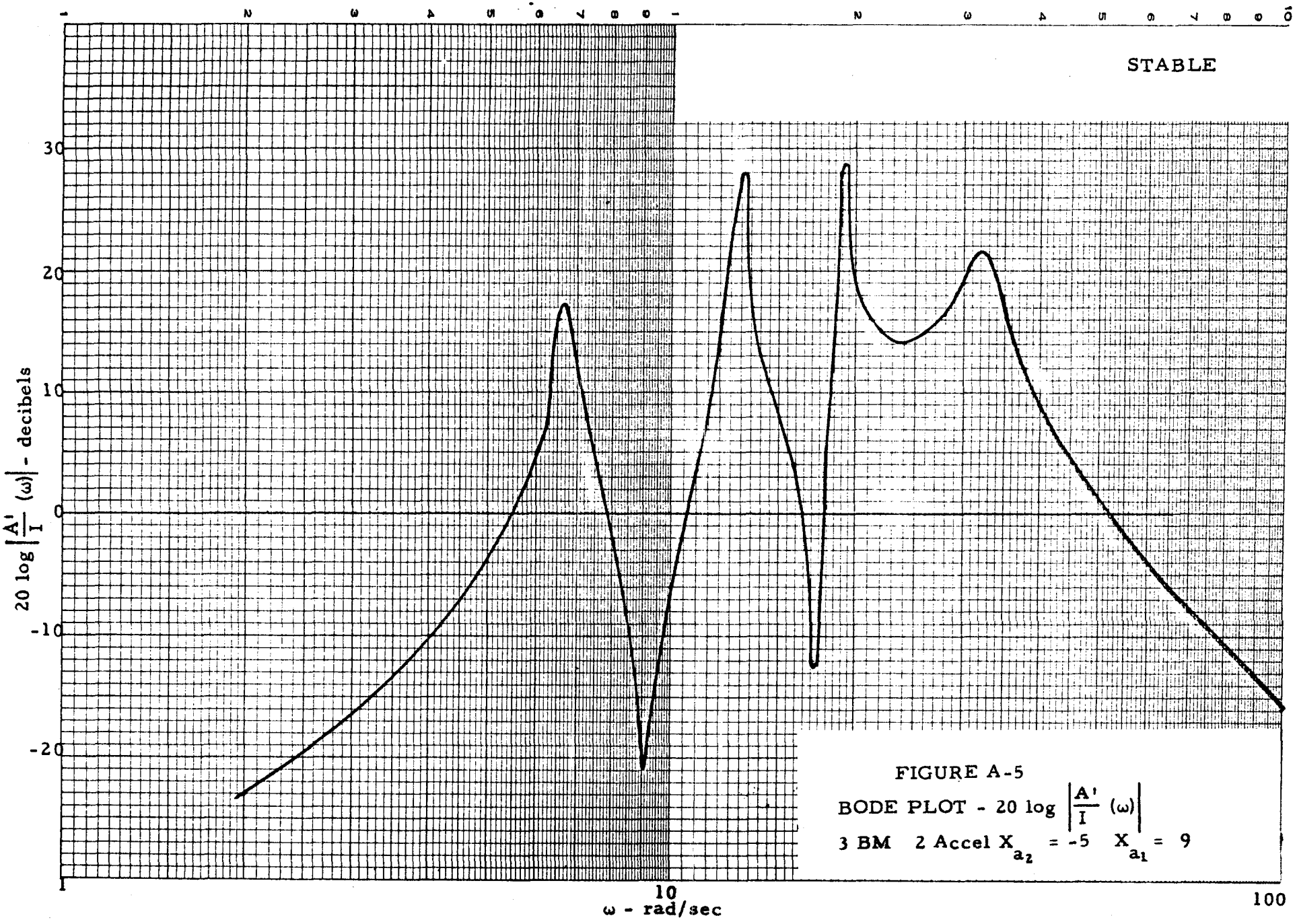


FIGURE A-5

BODE PLOT - 20 log $\left|\frac{A'}{I}(\omega)\right|$

3 BM 2 Accel $X_{a_2} = -5$ $X_{a_1} = 9$

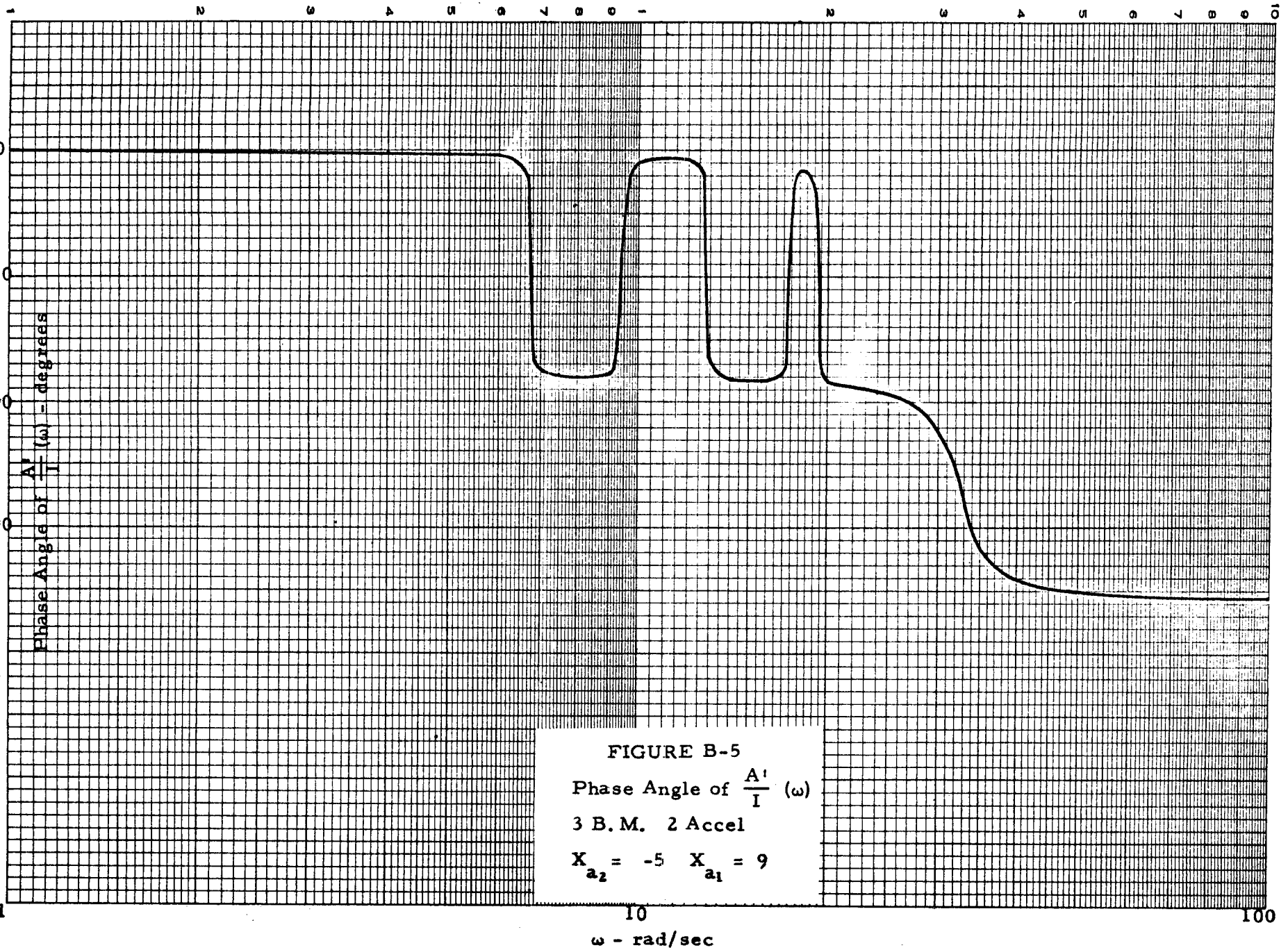


FIGURE B-5

Phase Angle of $\frac{A'}{I}(\omega)$

3 B. M. 2 Accel

$X_{a_2} = -5 \quad X_{a_1} = 9$

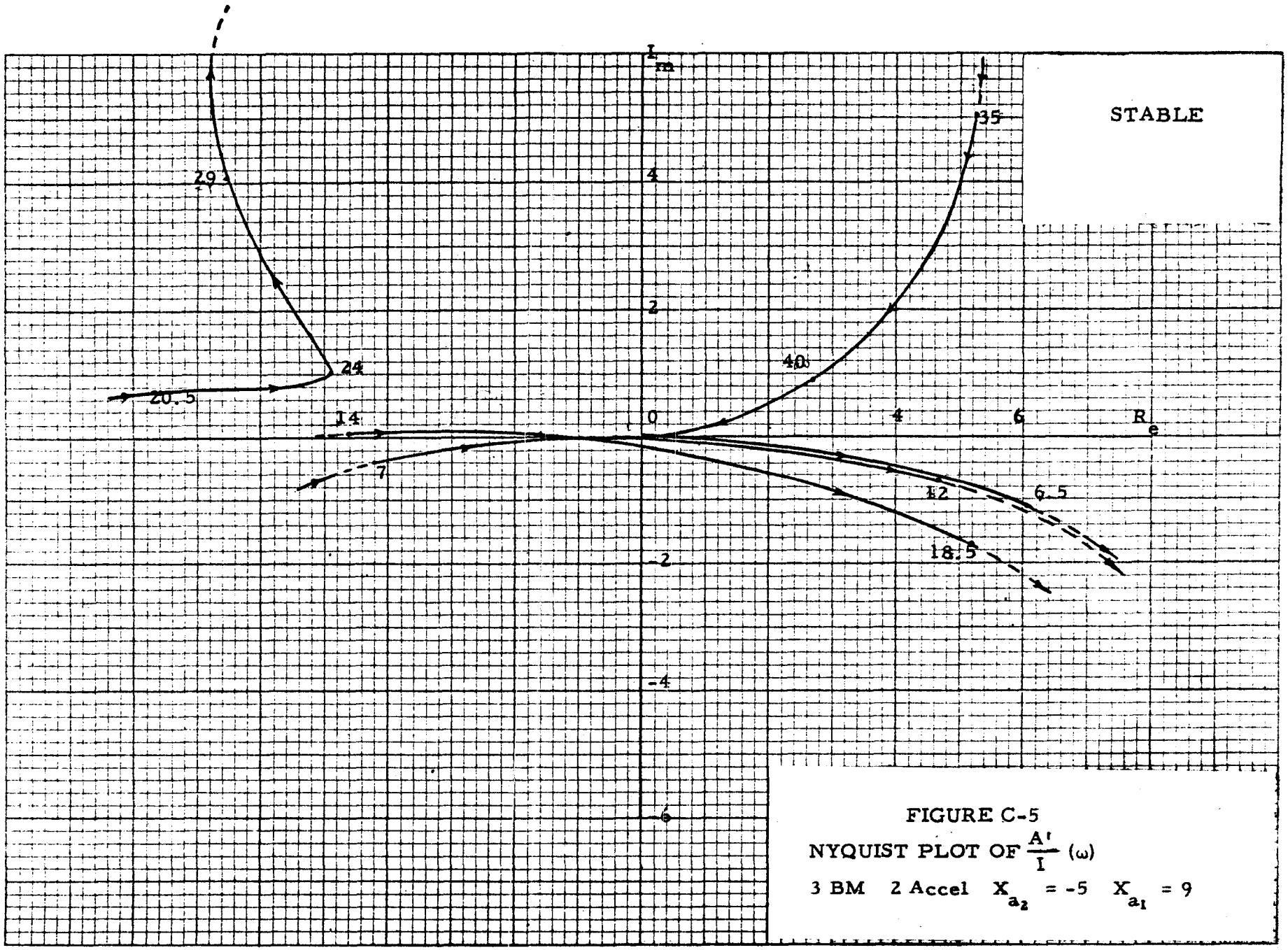


FIGURE C-5

NYQUIST PLOT OF $\frac{A'}{I}(\omega)$

3 BM 2 Accel $X_{a_2} = -5$ $X_{a_1} = 9$

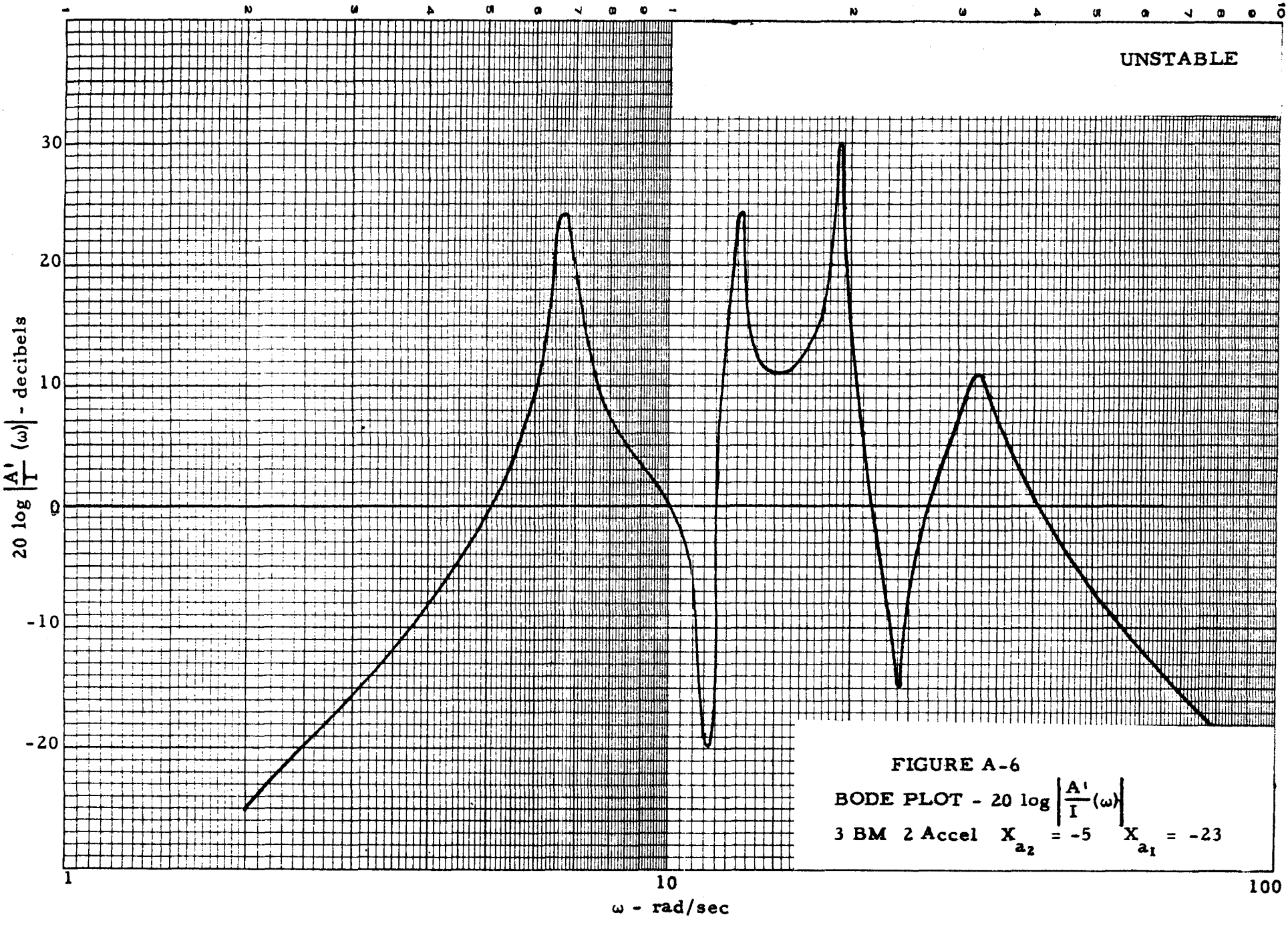


FIGURE A-6

BODE PLOT - 20 log $\left|\frac{A'}{I}(\omega)\right|$

3 BM 2 Accel $X_{a_2} = -5$ $X_{a_1} = -23$

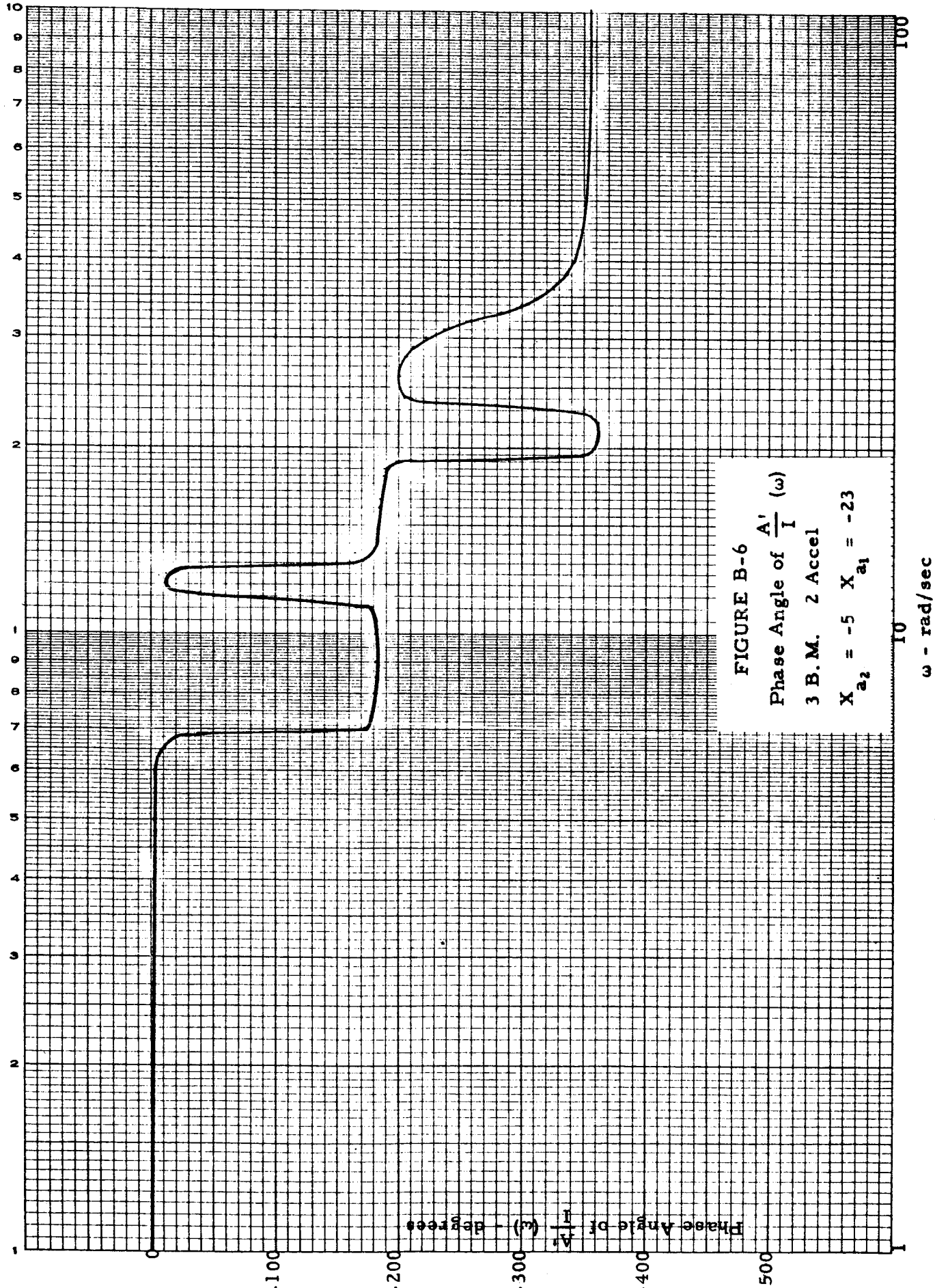


FIGURE B-6

Phase Angle of $\frac{A'}{I}(\omega)$

3 B.M. 2 Accel

$X_{a_2} = -5 \quad X_{a_1} = -23$

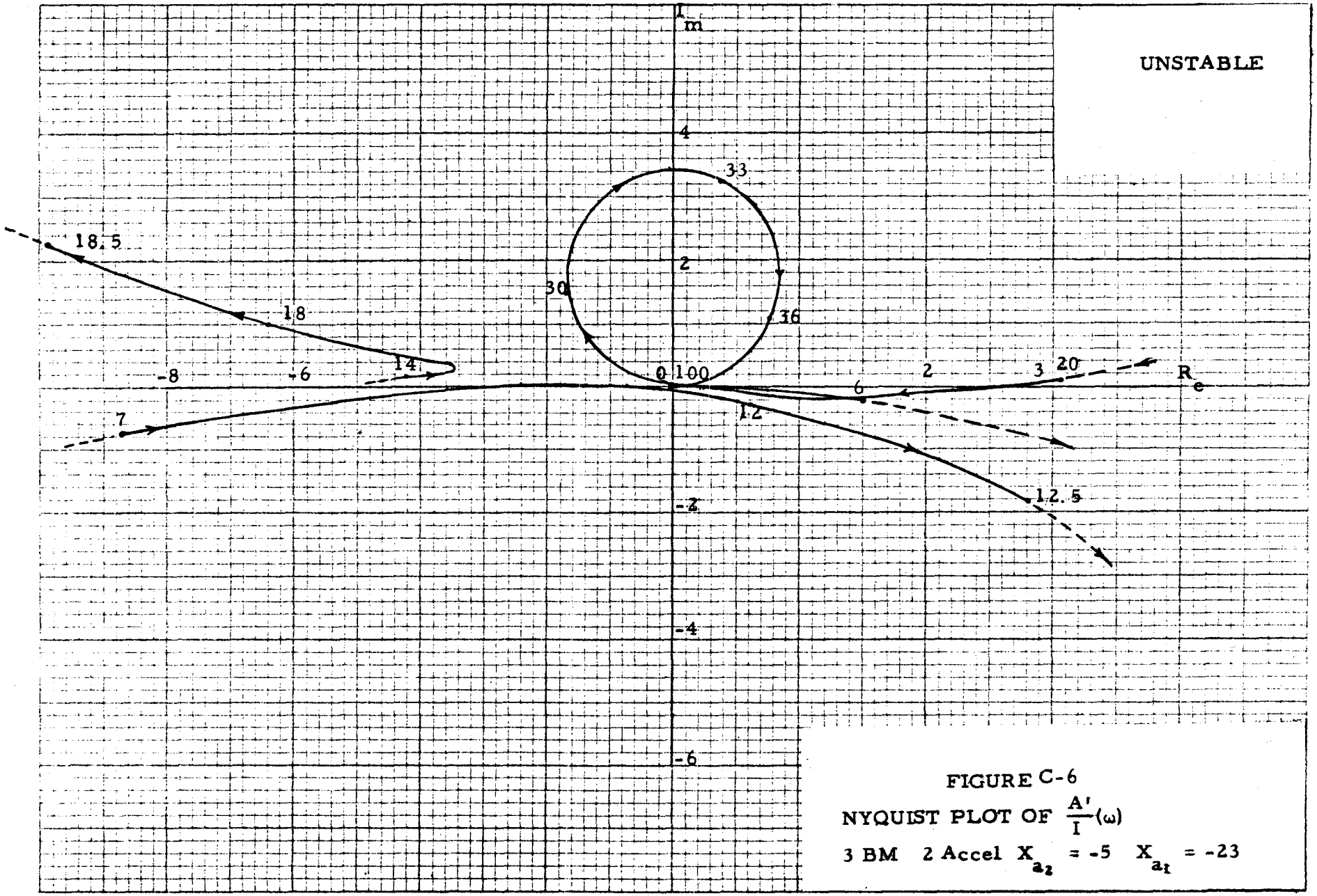


FIGURE C-6

NYQUIST PLOT OF $\frac{A'}{I}(\omega)$

3 BM 2 Accel $X_{a_2} = -5$ $X_{a_1} = -23$

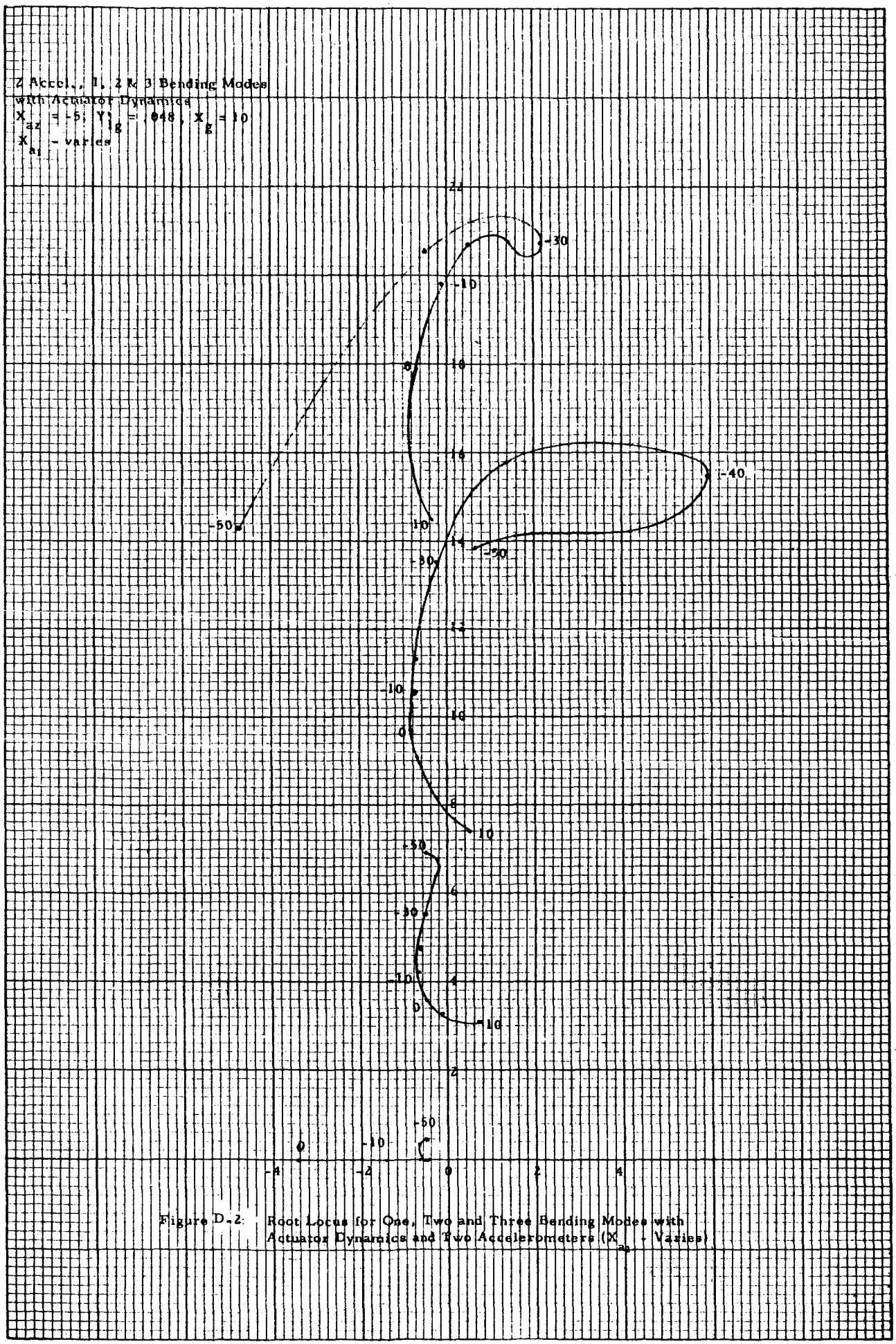
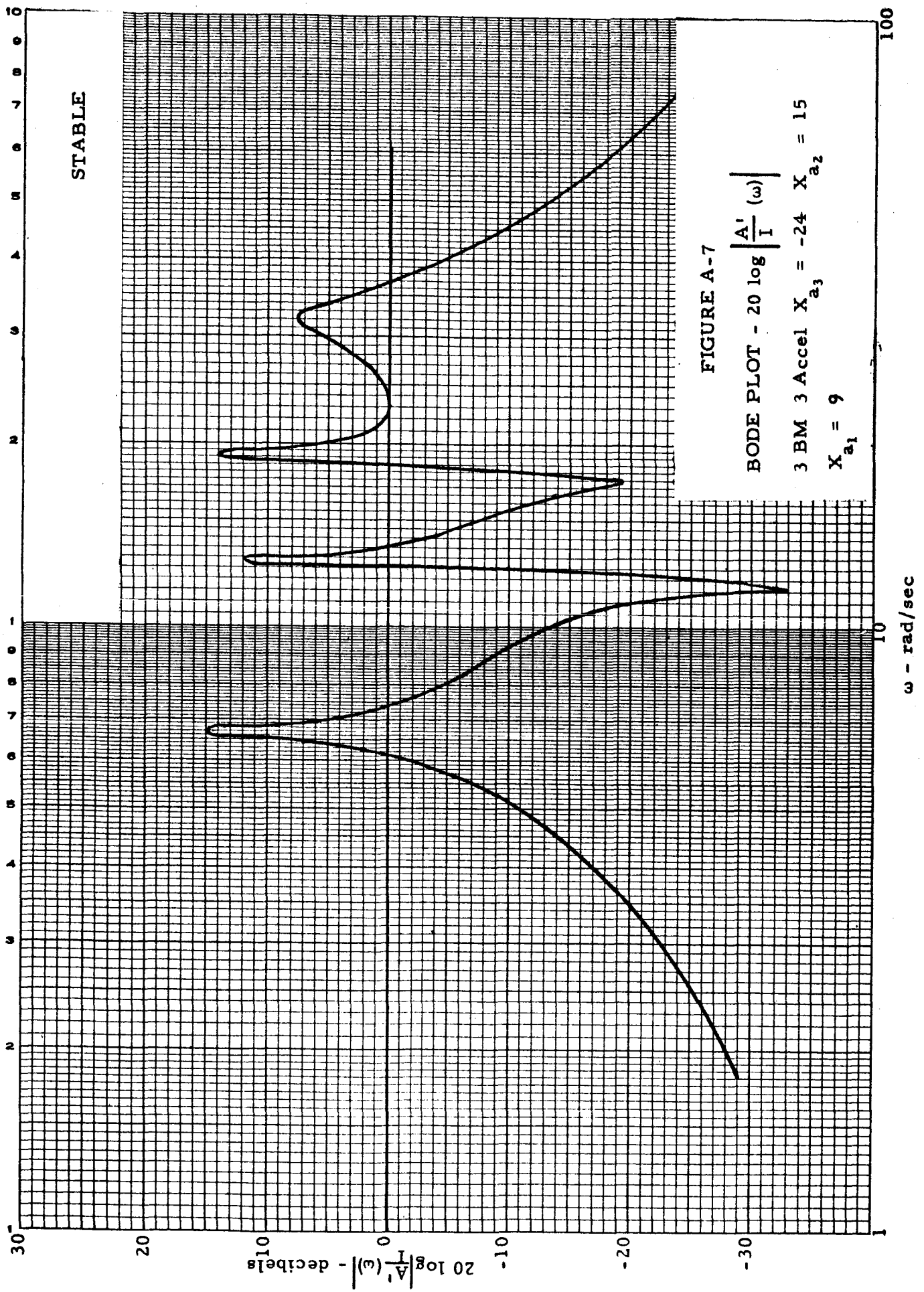


Figure D-2: Root Locus for One, Two and Three Bending Modes with Actuator Dynamics and Two Accelerometers (X_{ai} - Varies)


STABLE
FIGURE A-7
BODE PLOT - 20 log $\left|\frac{A'}{I}(\omega)\right|$
3 BM 3 Accel X_{a_3} = -24 X_{a_2} = 15
X_{a_1} = 9
20 log $\left|\frac{A'}{I}(\omega)\right|$ - decibels
ω - rad/sec
30
20
10
0
-10
-20
-30
1
10
100

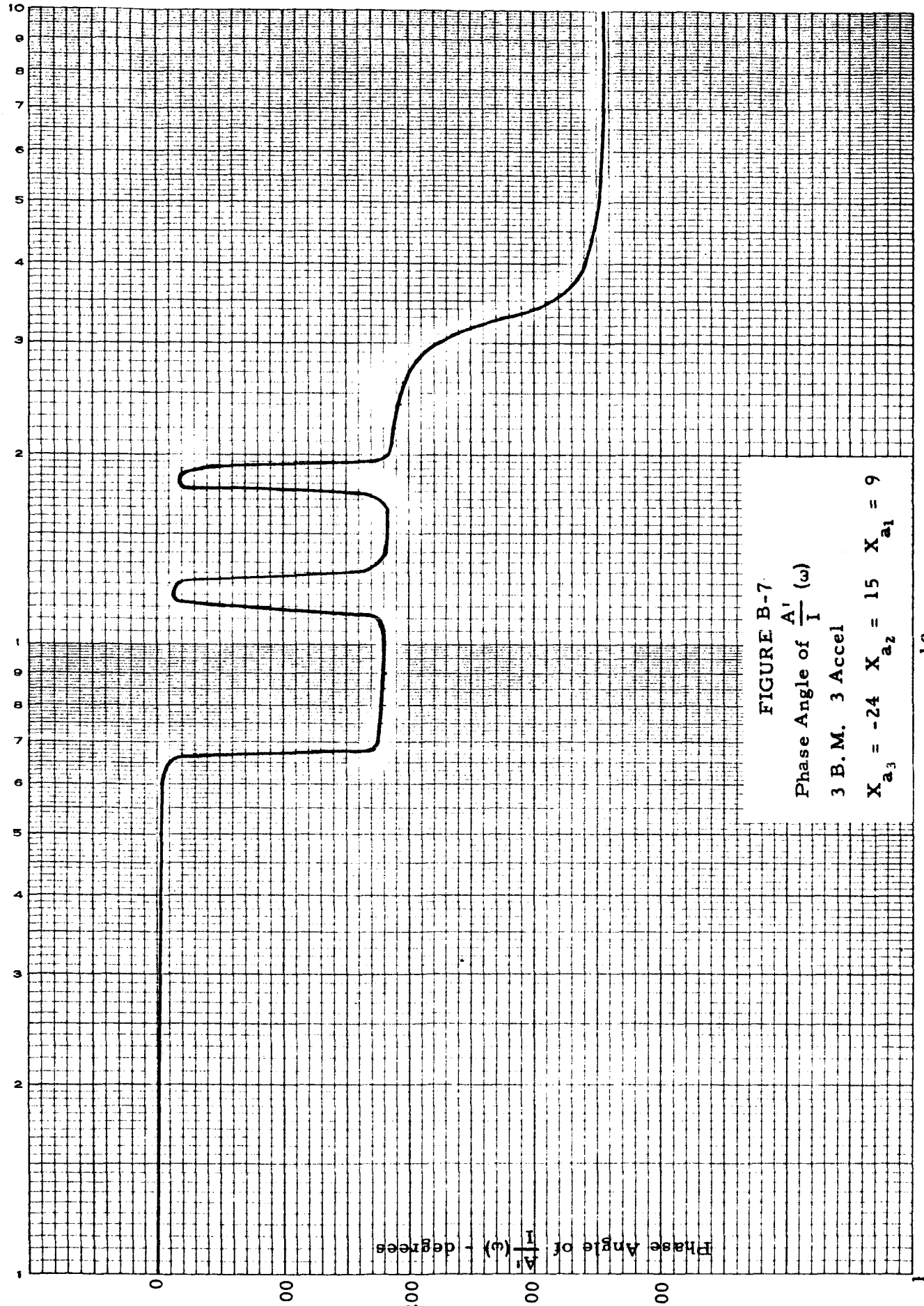


FIGURE B-7

Phase Angle of $\frac{A'}{I}(\omega)$

3 B.M. 3 Accel

$X_{a_3} = -24$ $X_{a_2} = 15$ $X_{a_1} = 9$

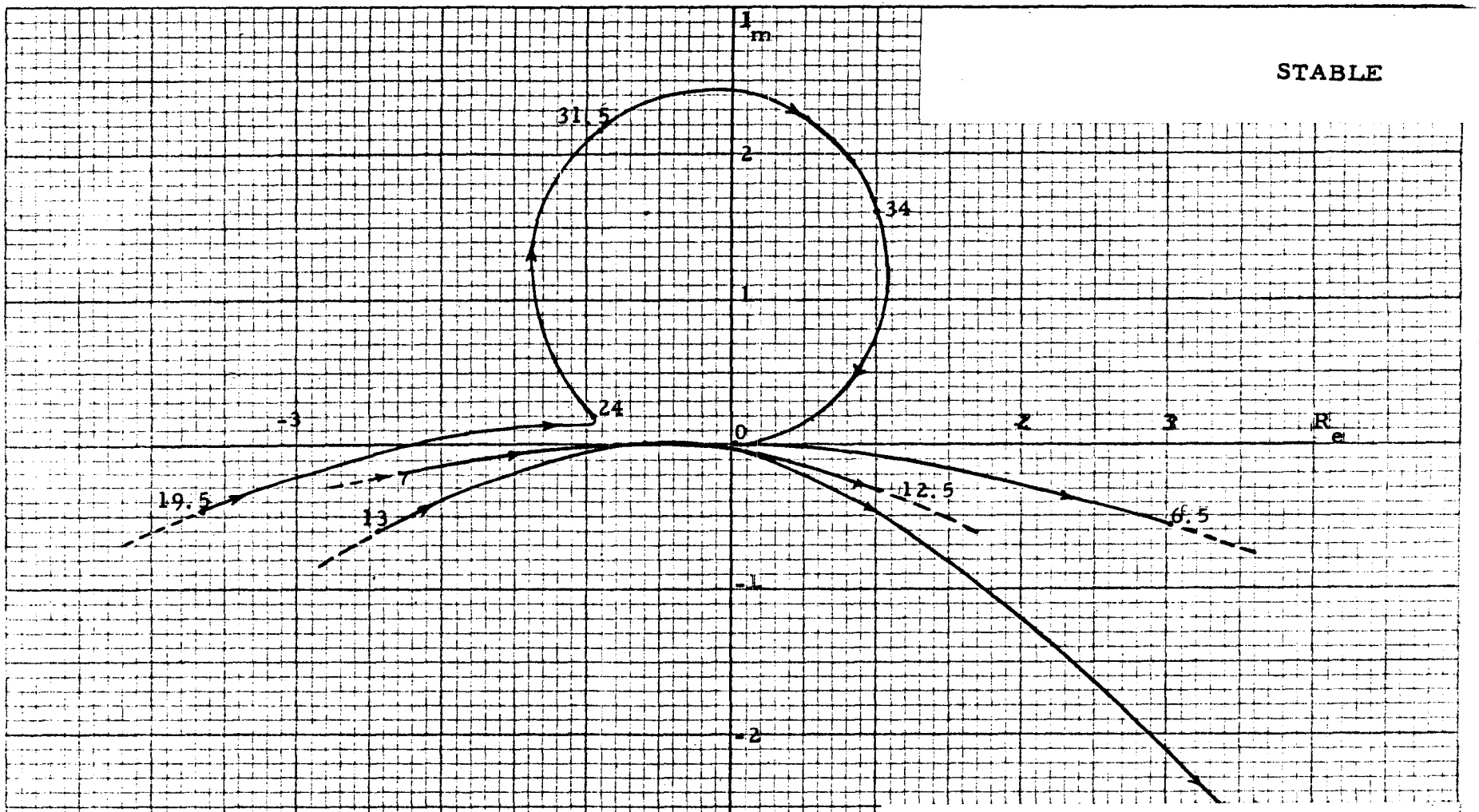


FIGURE C-7

NYQUIST PLOT OF $\frac{A'}{I}(\omega)$

3 BM 3 Accel $X_{a_3} = -24$ $X_{a_2} = 15$

$X_{a_1} = 9$

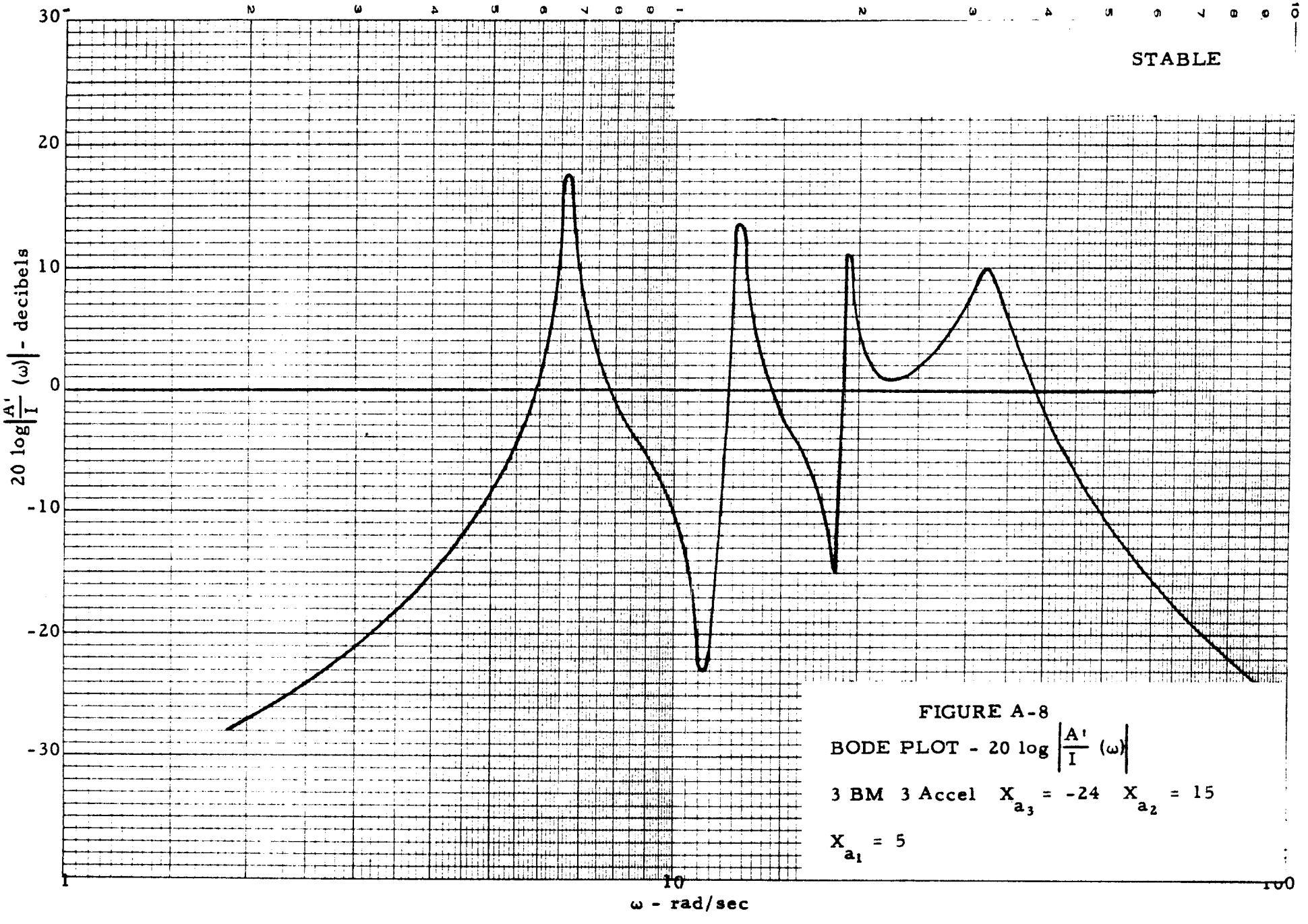


FIGURE A-8

BODE PLOT - 20 log $\left|\frac{A'}{I}(\omega)\right|$

3 BM 3 Accel $X_{a_3} = -24$ $X_{a_2} = 15$

$X_{a_1} = 5$

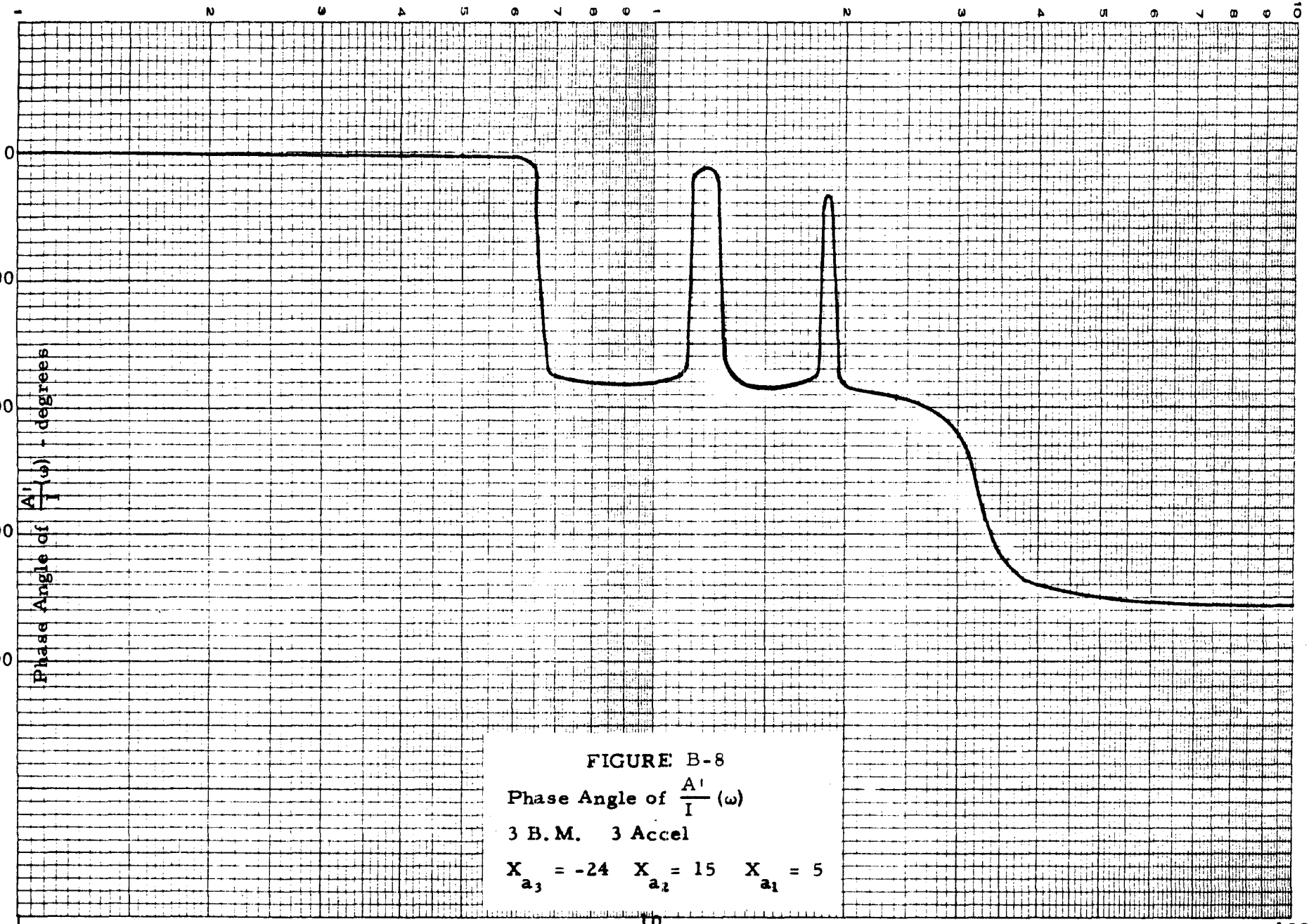


FIGURE B-8

Phase Angle of $\frac{A'}{I}(\omega)$

3 B.M. 3 Accel

$X_{a_3} = -24$ $X_{a_2} = 15$ $X_{a_1} = 5$

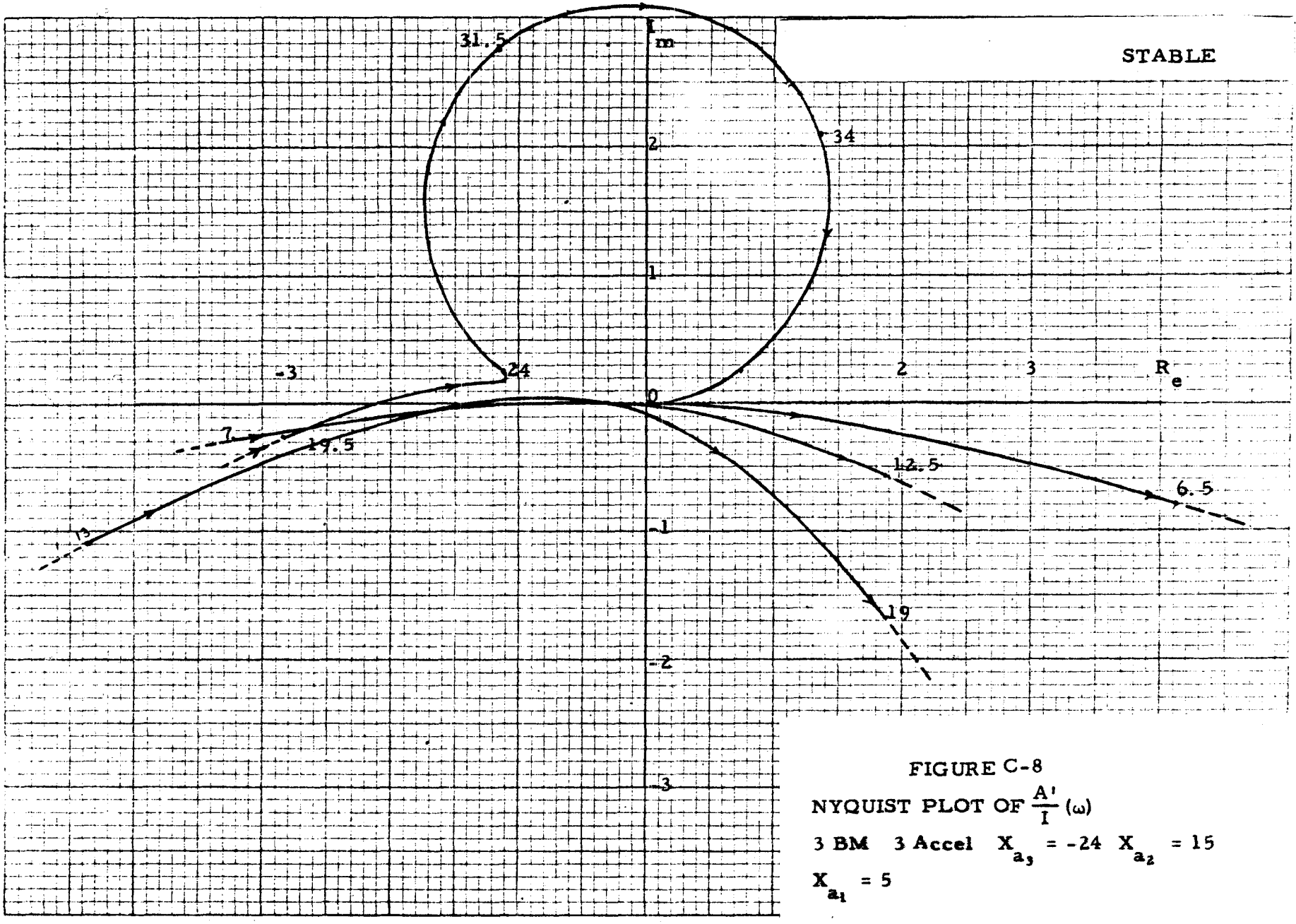


FIGURE C-8

NYQUIST PLOT OF $\frac{A'}{I}(\omega)$

3 BM 3 Accel $X_{a_3} = -24$ $X_{a_2} = 15$

$X_{a_1} = 5$

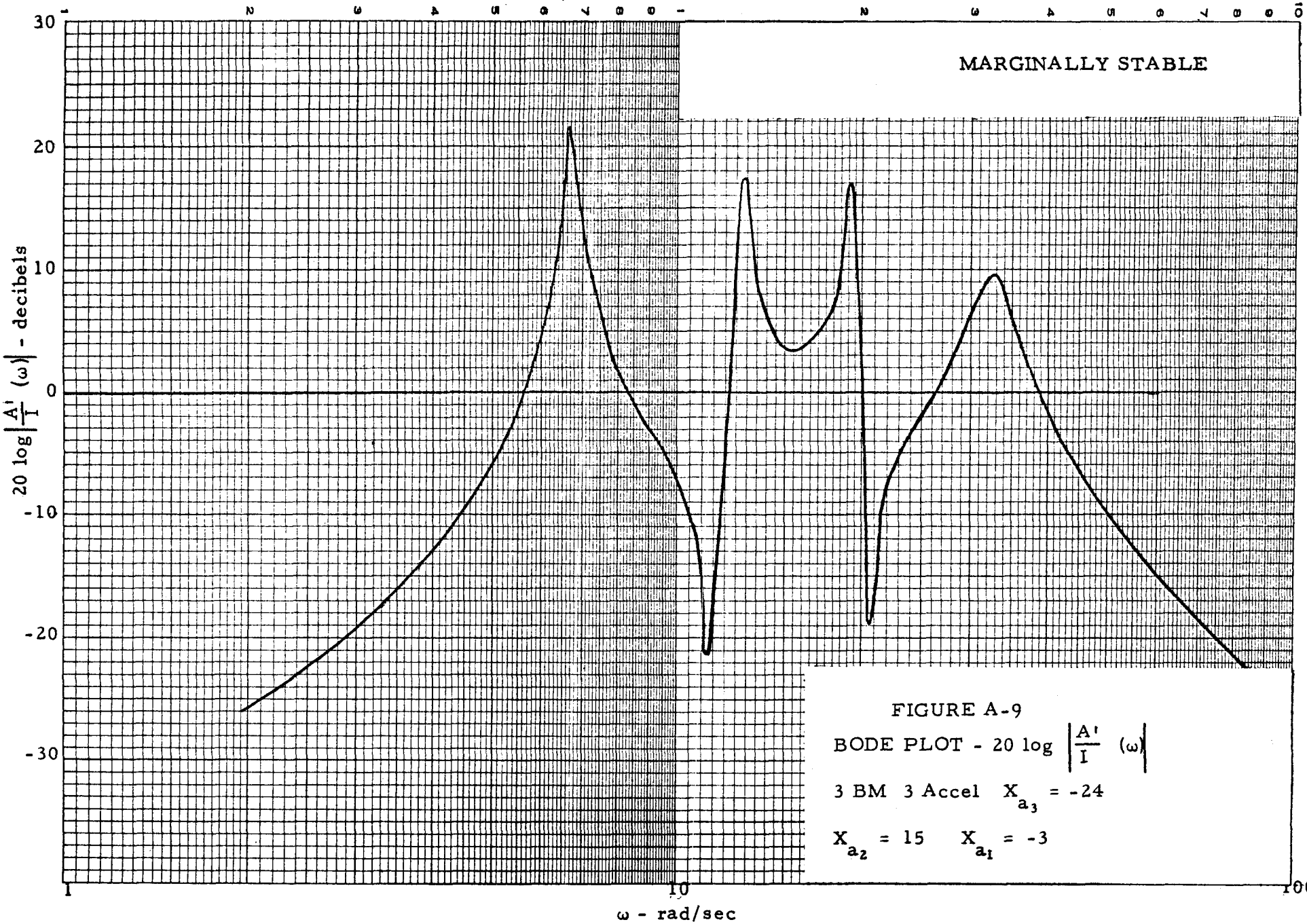


FIGURE A-9

BODE PLOT - $20 \log \left| \frac{A'}{I} (\omega) \right|$

3 BM 3 Accel $X_{a_3} = -24$

$X_{a_2} = 15$ $X_{a_1} = -3$

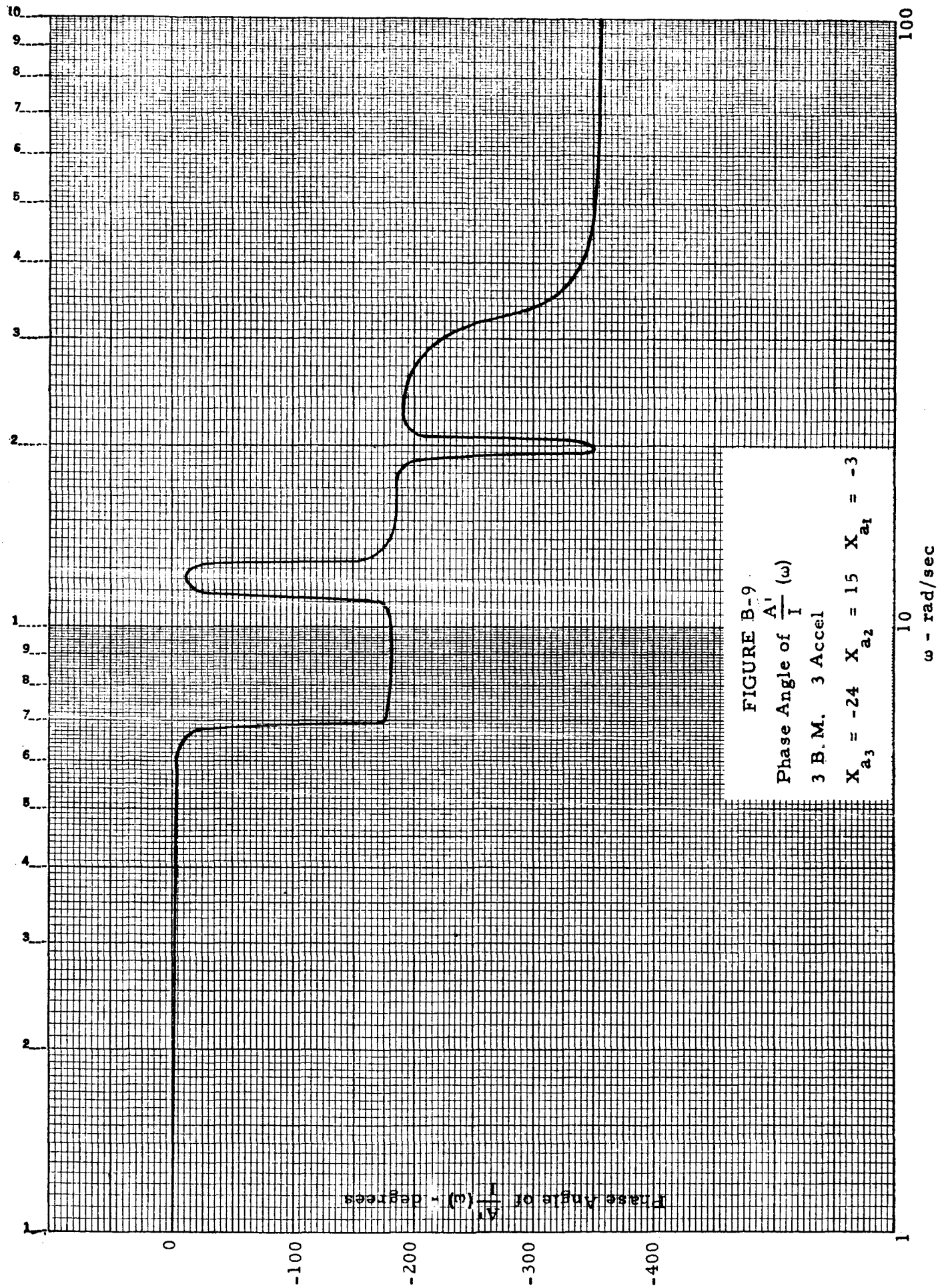


FIGURE B-9

Phase Angle of $\frac{A'}{I}(\omega)$

3 B.M. 3 Accel

$X_{a_3} = -24$ $X_{a_2} = 15$ $X_{a_1} = -3$

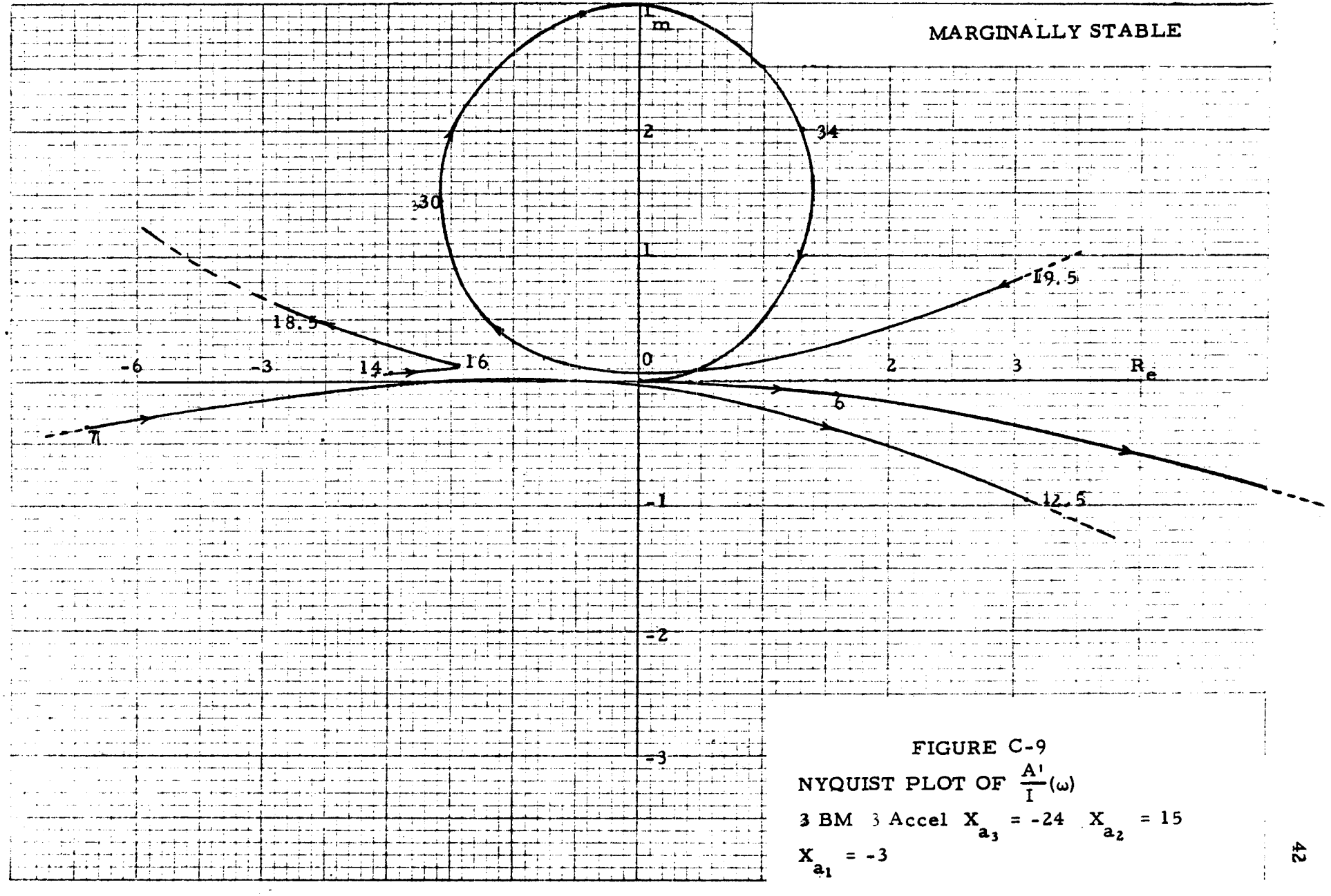


FIGURE C-9

NYQUIST PLOT OF $\frac{A'}{I}(\omega)$

3 BM 3 Accel $X_{a_3} = -24$ $X_{a_2} = 15$

$X_{a_1} = -3$

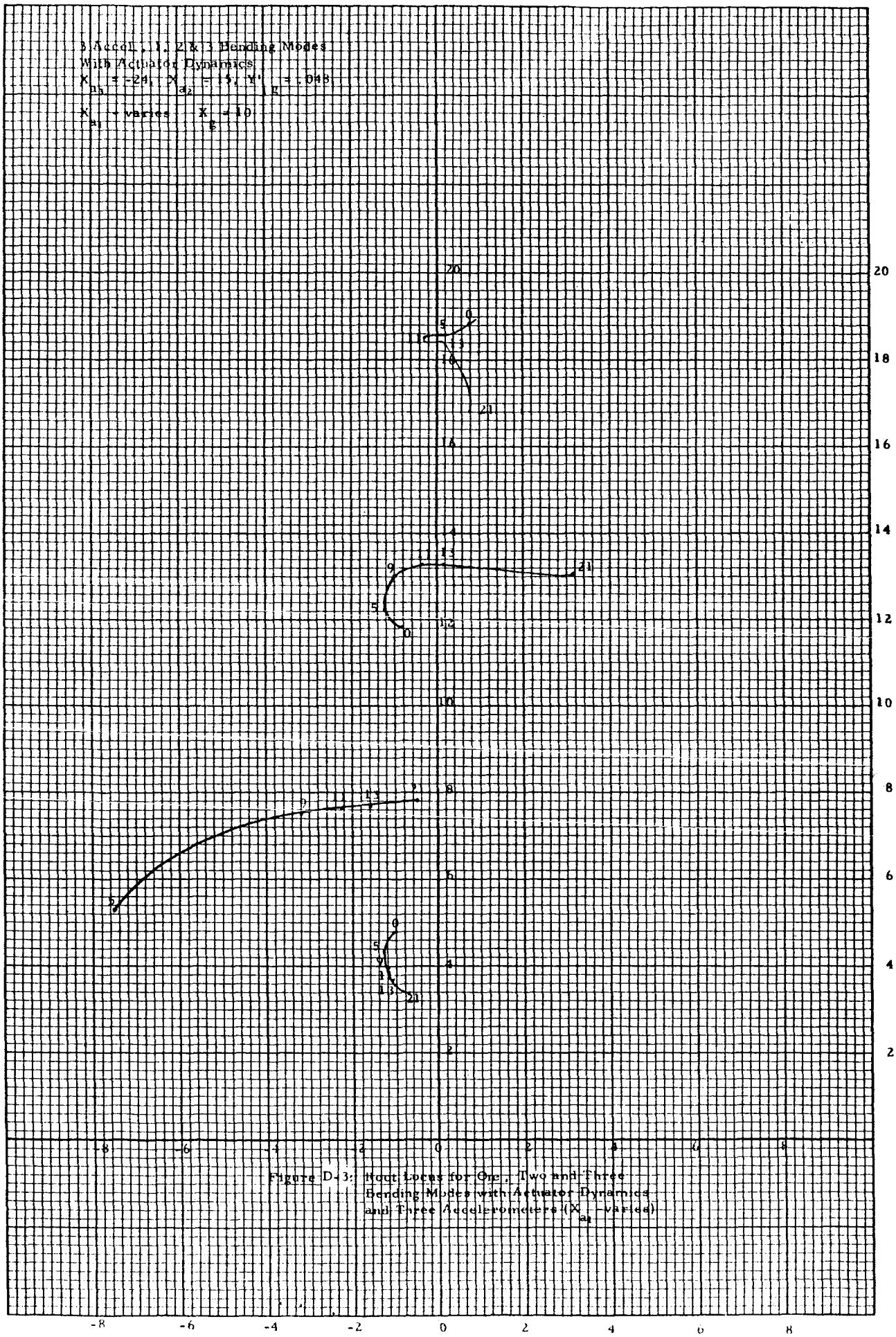


Figure D-3: Root Locus for One, Two and Three Bending Modes with Actuator Dynamics and Three Accelerometers (X_{a_1} varied)